UNIVERSITY OF BIRMINGHAM

Characterisation of Anode Supported Microtubular SOFC Process on Pure Methane Reduction and Operation

by

Tae Jung Lee

A thesis submitted to
The University of Birmingham
For the degree of

DOCTOR OF PHILOSOPHY

Chemical Engineering
School of Engineering
University of Birmingham
Edgbaston
Birmingham
United Kingdom
B15 2TT
2009

Acknowledgements

Firstly, I would like to thank Prof. Kevin Kendall, my supervisor, for allowing me to undertake a project under his supervision.

I would like to thank my supervisor, Prof. Oh Young Kim, at Dankook University for his support and advice. Also thanks to my colleagues and friends in Korea.

I would like to thank my colleagues and friends who guide me, Dr Christian Mallon, Dr Aman Dhir and Dr Chinnan Dikwal.

Finally I dedicate this thesis my family for their encouragement and support throughout the period of study.

ABSTRACT

The optimisations of reduction and operation of Ni-YSZ anode supported micro tubular solid oxide fuel cells (SOFC) on pure methane were studied.

A major problem of SOFCs is nickel anode performance on methane and higher hydrocarbons [1]. The aim of this work was to study the effect of reduction and operation of anode-supported microtubular SOFCs using methane as both reductant and fuel. The results were compared to those from optimised operation using hydrogen. To measure mechanical strength, the three point bending test was employed. Temperature programmed oxidation (TPO) results were investigated to measure the carbon deposition on the anode in order to assess potential damage to the cermet catalyst. Also field emission scanning electron microscope (FE-SEM) and Energy-Dispersive X-ray spectroscopy EDS results were analysed on the anode surface.

In hydrogen operation, the value of tube fracture force in bending was found to lie between 102MPa and 137MPa after 1 hr reduction with 20ml/min of hydrogen at 750 °C. The micro-tubular cell showed the highest current density of 1.38 A/cm^2 at 850 °C using the optimization point of 850°C reduction temperature and 20ml/min hydrogen. From the results, it was clear that the performance could be substantially improved by optimising reduction conditions.

In methane, the micro tubular SOFCs were both reduced and operated under various conditions, in contrast to previous literature where the cell was reduced in hydrogen and subsequently operated on methane [2-4]. Results showed that carbon deposition was minimized after certain reduction conditions. The conclusion was that 30 minutes reduction at 650℃ with 10 ml/min methane flow rate led to the highest current output over 1.45 A/cm^2 at 0.5 V when the cell operated at 850℃ with 10ml/min methane running flow rate. 45 minutes showed the best mechanical strength while reduction and operation on methane was shown to give performance benefits, eliminating the need for additional hydrogen infrastructure. From these results, it is evident that SOFC performance can be substantially improved by optimizing preparation, reduction and operating conditions without the need for hydrogen. This advance will benefit domestic SOFC users because hydrogen is not yet available in homes throughout the world.

.

CONTENTS

FIGURES

TABLES

Chapter 1

Introduction

1.1 Fuel Cell Description

Fuel cells got their start when William Grove immersed two platinum strips surrounded by closed tubes containing hydrogen and oxygen in an acidic electrolyte back in 1839 [5]. Basically, fuel cells take advantage of the innate nature of hydrogen and oxygen gases to form water when they are either heated or a catalyst is added. This electrochemical reaction takes place at anode and cathode, separated by electrolyte membrane, releasing electricity and heat energy.

Thus a fuel cell is a device that converts the chemical energy of a fuel (hydrogen, natural gas, methanol, gasoline, etc.) and an oxidant (air or oxygen) into electricity. The basic components of an oxide based fuel cell are shown in Figure 1.1. In principle, a fuel cell operates like a battery. Unlike a battery however, a fuel cell does not run down or require recharging. It will produce electricity and heat as long as fuel and an oxidizer are supplied [6-8]. There are several different types cells described in table 1.1

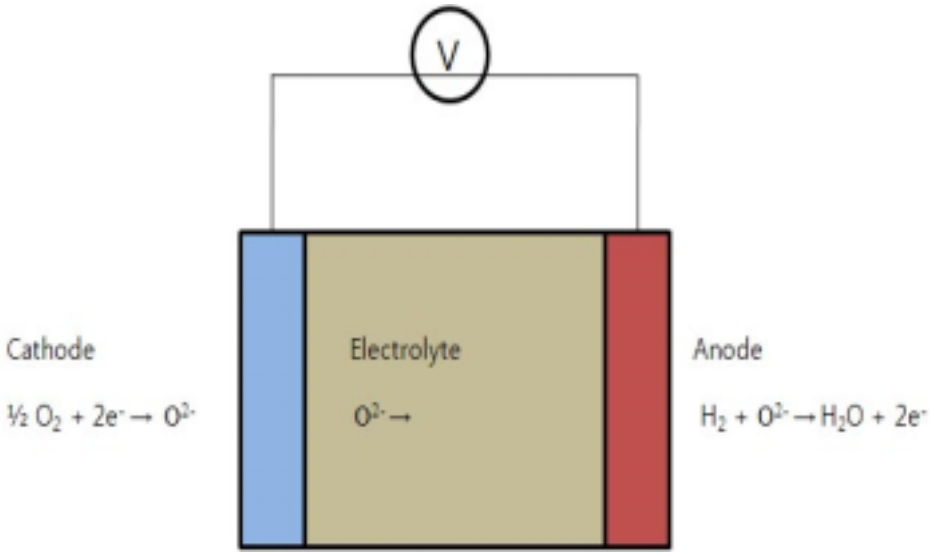

Figure 1.1: General operating principle of an oxide based fuel cell

A number of different types of fuel cell are being developed. The characteristics of each type vary mainly in electrolyte and electrode, but also in terms of operating temperature, power density, available heat and tolerance to thermal cycling and tolerance to fuel impurities. These differences make each technology suitable for particular applications. They are also at very different stages of development. Some have not yet emerged from the laboratory.

All of these technologies could achieve significant market share in competition with conventional alternatives such as combustion engines: that is if they become technically mature on the one hand, and on the other can be produced at costs required to be competitive for their particular application. The major difference in fuel cell designs has to do with the electrolyte. Some fuel cells have

aqueous electrolyte, some molten, while others are solid ceramics or polymers. Differences in electrolyte material also affect the applications and manufacturing costs of a fuel cell [9].

1.2 Types Of Fuel Cell

Basically, there are four main types of fuel cells shown in Table 1.1. They differ in the composition of the components and are in different stages of development.

Features	Cell Types			
Cell Name	Polymer electrolyte	Phosphoric acid	Molten carbonate	Solid oxide
Operating temperature	70 – 90 °C	180 – 220 °C	650 – 700 °C	800 – 1000 °C
Charge carrier	H^+	H^+	CO_3^{2-}	O^{2-}
Catalyst, Anode	Platinum (Pt)	Platinum (Pt)	Nickel (Ni)	Nickel (Ni)
Fuel	H^+	H^+	Reformate or CO/H^+	Reformate or CO_2/H_2 or CH_4
Reforming	External or MeOH	External	External or Internal	External or Internal direct CH_4
Cell efficiency	40 – 50	40 – 50	50 – 60	50 – 60
Co-generation heat	None	Low quality	High	High
Oxidant for fuel cell	O_2/air	O_2/air	CO_2/O_2/air	O_2/air

Table 1.1: Fuel cells features [10]

They are phosphoric acid fuel cell (PAFC), proton-exchange membrane fuel cell (PEMFC), molten carbonate fuel cell (MCFC), and solid oxide fuel cell. Table 1.1 shows the main features of the four main types of fuel cells summarized from recent publications [10-12].

All fuel cells work on similar principles. They are continually supplied with fuel and oxidant, usually air. These are supplied to separate electrodes where they are then converted into electrons and ions. The ions travel through an ion conducting membrane (the direction of travel depends on the type of cell). The electrons travel through an external circuit to supply power.

1.2.1 Proton Exchange Membrane Fuel Cell (PEMFC)

The use of organic cation exchange membrane as a solid electrolyte in an electrochemical cell was originally devised by William T. Grubb in 1959 [12].

The basic cell consists of a proton conducting membrane, such as a perfluorinated sulfonic acid polymer, sandwiched between two platinum impregnated porous electrodes. The back of the electrodes is made hydrophobic by coating with an appropriate compound. This wet proof coating provides a path for gas diffusion to the catalyst layer. The standard electrolyte material

presently used in PEFCs is a fully fluorinated Teflon-based material, Nafion produced by E.I. Du Pont for space application in the mid-1960s [13].

Because of the limitation on the temperature imposed by the polymer and water balance, the stack runs at a relatively low temperature of 80 °C (176 °F). Additional problems of the PEM system are high manufacturing costs and complex water management issues. The stack contains hydrogen, oxygen and water. If dry, the input resistance is high and water must be added to get the system going. Too much water causes flooding. Freezing can also damage the stack. The warm-up is slow and the performance is poor when cold. The cooling systems are expensive [10].

The PEM system allows compact designs and achieves a high energy to weight ratio. Another advantage is a quick start-up when hydrogen is applied. The efficiency is approximately 50 %. In comparison, the internal combustion motor has an efficiency of about 25%. The PEMFC technology is primarily suited for residential commercial and business transportation application [14-16].

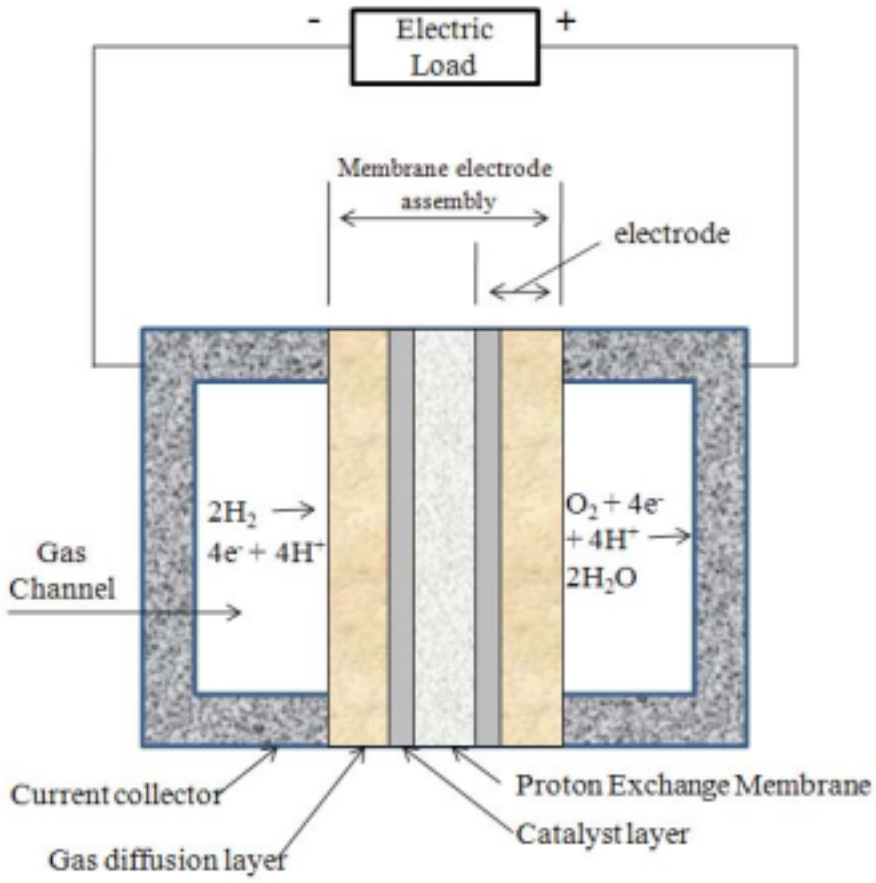

Figure 1.2 Operating principle of the Proton Exchange Membrane Fuel Cell [15]

The electrochemical reactions of PEFC are similar to those of the PAFC: hydrogen at the anode provides a proton, freeing an electron in the process that must pass through an external circuit to reach the cathode. The proton, which remains solvated with a certain number of water molecules, diffuses through the membrane to the cathode to react with oxygen and the returning electron [17]. Water is subsequently produced at the cathode.

1.2.2 Molten Carbonate Fuel Cell (MCFC)

In the mid-1960s, this high temperature molten salt technology evolved to use Ni-based alloy at the anode and oxide at the cathode. Since the mid-1970s, the materials for the electrodes and electrolyte structure have remained essentially unchanged.

A major development in the 1980s was the evaluation in the technology for fabrication of electro structures. Molten Carbonate fuel cells operate at temperatures between 500°C and 800°C and are often referred to as medium temperature fuel cells [20].

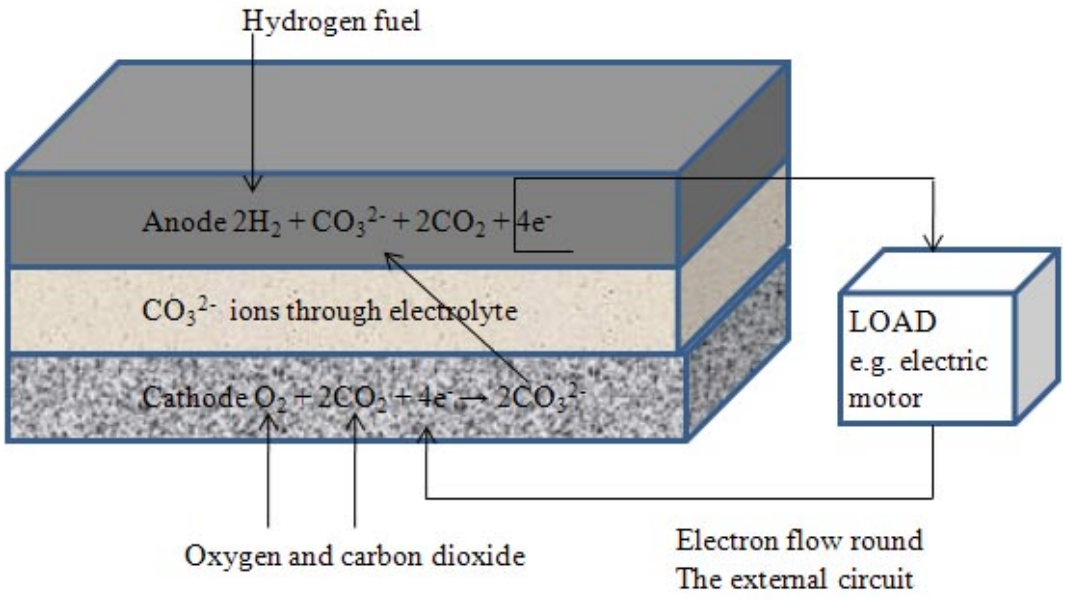

Figure 1.3 Operating principle of the molten carbonate fuel cell [20]

The electrolyte in this fuel cell is usually a combination of alkali carbonates, retained in a ceramic matrix. The cathode reaction is similar to that in alkaline fuel cells, but instead of oxygen combining with water, it combines with carbon dioxide, picking up electrons from the external circuit [20]. This is illustrated schematically in Figure 1.3

The electrochemical reactions occurring in MCFCs are

$$2H_2 + 2CO_3^{=} \rightarrow 2H_2O + 2CO_2 + 4e^-$$

at the anode, and

$$O_2 + 2CO_2 + 4e^- \rightarrow 2CO_3^{=}$$

at the cathode. The overall cell reaction is

$$2H_2 + O_2 + 2CO_2\,(\text{Cathode}) \rightarrow 2H_2O + 2CO_2\,(\text{anode})$$

1.2.3 Phosphoric Acid Fuel Cell (PAFC)

A diagram showing the operating principles of the phosphoric acid fuel cell (PAFC) is shown in Figure 1.4. In the mid-1960, the conventional porous electrodes were polytetra-fluoroethylene (PTFE)-bond Pt black, with loading of

9mg Pt/cm^2. During the past two decades Pt supported on carbon black has replaced Pt black in porous PTFE-bonded electrode structures as a catalyst. Platinum supported on porous carbon is used on both the anode and cathode sides of the electrolyte. The PAFC operates at 180-220°C, typically around 200°C in 100% H_3PO_4. Operating at 200°C, the PAFC plant produces heat for domestic hot water and space heating. PAFC is the most mature fuel cell technology in terms of system development and is already in the first stages of commercialisation [21]. PAFC power plant design can achieve 40 – 45% fuel-to-electricity conversion efficiencies on lower heating value basis.

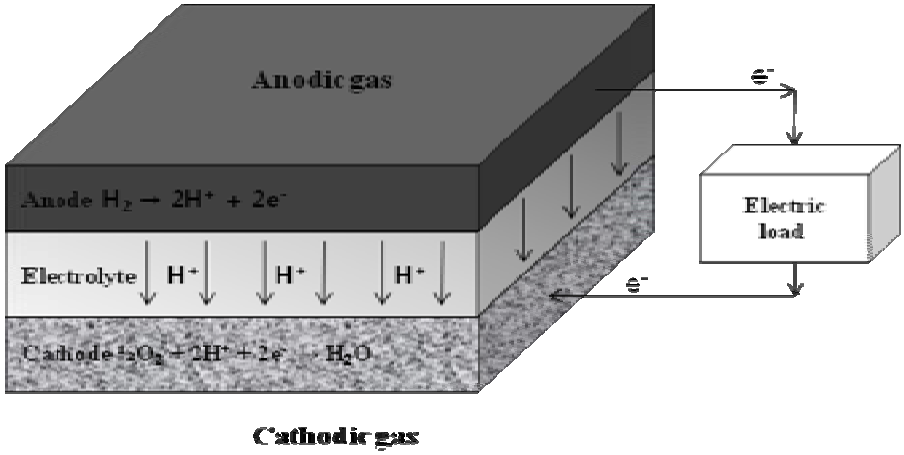

Figure 1.4 Operating principle of the phosphoric acid fuel cell [22]

The electrochemical reactions occurring in PAFCs are

$$H_2 \rightarrow 2H^+ + 2e^-$$

At anode, and

$½O_2 + 2H^+ + 2e^- \rightarrow H_2O$

at the cathode. The overall cell reaction is

$½O_2 + H_2 \rightarrow H_2O$

1.2.4 Solid Oxide Fuel Cell (SOFC)

Solid oxide fuel cells (SOFCs) have grown in recognition as a viable high temperature fuel cell technology. SOFCs consist entirely of solid-state materials. They utilize a fast oxygen ion conducting ceramic as the electrolyte, and operate in the temperature range of 500 – 1000°C.

SOFCs have several features that make them more attractive than other types of fuel cells:

- The highest efficiencies of all fuel cells (50- 60%)
- A potential long-life expectancy of more than 40,000 – 80,000 h.
- Constructed from readily obtainable ceramic materials, not precious metals like platinum

- High grade waste heat is produced, for combined heat and power (CHP) application increasing over-all efficiencies to over 80%
- Internal reforming of hydrocarbon fuels is possible

Conventional high temperature SOFCs designed by Westinghouse or Rolls Royce operate at around 950°C. This temperature implies high costs, particularly for interconnect and construction materials. Operation of the SOFC at a reduced temperature can overcome some those problem and bring additional benefits [23].

- Low-cost metallic materials make both the stack and balance of plant cheaper and more robust
- Potential for rapid start-up and high capability of thermal cycle
- Simplification of the design and materials requirements of the balance of plant
- Significant reduction of corrosion rates, higher long-term stability of

the system.

However, the SOFC is still in the developmental stage and will not be available for commercial applications for several years. Since there are several ceramic layers involved, their properties must be compatible. The materials can only be used in compatible sets, and a change in one component may have negative consequences for other parts of the cell. Many SOFC materials and fabrication problems would be reduced if a lower temperature oxide ion conductor were available.

Developing electrolytes that are alternatives to zirconia would extend the operating life of SOFCs and ensure a shorter heating time before start up. Though material properties can be manipulated to compensate for these drawbacks, introducing a new electrolyte sacrifices compatibility with other materials [21, 24-26].

In this range of operation temperature (500 – 1000°C), carbon monoxide can also act as a fuel besides hydrogen in SOFC. Hydrocarbons such as methane can also be oxidised at the anode but carbon deposition can cause severe damage under certain operating conditions [27]. The purpose of this thesis is to investigate this carbon deposition problem in more detail.

The SOFC electrolyte that separates the anode and cathode is an oxygen-ion-conducting material. On the cathode side (air electrode) side, oxygen atoms react with incoming electrons from external load to become oxygen ions which move through the electrolyte. On the anode (fuel electrode) side, fuel is oxidized by incoming oxygen ions to liberate the electrons that flow through the external electrical circuit.

The electron flow in the external circuit is balanced by ionic current flow within the electrolyte. More specifically, if the electrolyte conducts oxide ions, oxygen will be electro-reduced at the cathode to produce O^{2-} ions and consume electrons, whereas oxide ions, after moving across the electrolyte, will react at the cathode with hydrogen and release electrons [25-29]: A typical SOFC is comprised of a fully dense layer capable of conducting oxygen ions, and electrically conducting, porous anode and cathode layers as shown in Figure 1.1.

At present, a cermet consisting of Ni-metal and Y_2O_3-stabilized ZrO_2 (YSZ) is widely used as an anode material in high temperature SOFCs [29-31]. This material is preferred because of its good electronic conductivity, chemical and structural stability, catalytic properties and compatibility with other materials in SOFCs [29]. YSZ is usually the electrolyte. The cathode is usually to connect

SOFCs into stacks, inter-connectors are used to make parallel and/or series connections between individual cells.

When hydrogen fuel is supplied to the cell for the first time, NiO-YSZ is converted into Ni-YSZ cermet. As a result of NiO reduction into Ni-metal the volume and porosity of the anode layer change, as well as other physical and mechanical properties. The initial reduction process introduces mismatch stress in multi-layered SOFC components, which in turn could have effects on the reliability and structural integrity of SOFCs [32].

The electrochemical reactions occurring in SOFCs utilizing H_2 and O_2 are based on equations:

$H_2 + O^{=} \rightarrow H_2O + 2e^-$

at the anode, and

$½O_2 + 2e^- \rightarrow O^{=}$

at the cathode.

Overall cell reaction is

$H_2 + ½O_2 \rightarrow H_2O$

1.3 Fuel

Hydrogen is the current fuel of choice for all fuel cells, though other hydrogen-rich molecules are popular because they are more readily available. Other gases, such as CO and methane CH_4, have different effects on fuel cells, depending on the type of fuel cell. Each fuel cell with its specific electrolyte and catalysts will accept different gases as fuels and experience poisoning or dilution [12]. Therefore, the gas supply systems must adapt to a specific type of fuel cell. Fuel cells can be poisoned by different types of molecules. Because of the difference in electrolyte, operating temperature, catalyst and other factors, different molecules can behave differently in different fuel cells. In particular, where nickel cermet is used for the anode, carbon from CO and methane can cause damage, eventually poisoning the cell.

Another major poison for all types of fuel cells is sulfur-containing gas such as hydrogen sulfide (H_2S) or carbonyl sulfide (CoS) [33-37]. Sulfur compounds are naturally present in all fossil fuels, and small quantities remain after normal processing and must be almost completely removed prior to entering the fuel cell.

1.4 Thesis aims

The object of the work is to study the direct injection of methane into SOFC

anodes in micro-tubular cells. The key aim is to be able to operate all processes from reduction to operation on methane without cell failure from carbon deposition. The reason for this study is the wide availability of methane, especially in pipeline gas, whereas hydrogen is not generally so easily accessed.

The cells were tested using a variety of conditions to determine the optimum for methane. Chapter 2 starts by taking a review of SOFC technology, from materials to design. Chapter 3 gives the testing practices and methods used throughout the experimental chapters. Chapter 4 examines micro tubular fuel cell optimisation for reduction and operation conditions using various flow parameters on hydrogen. Also the influence of methane reduction conditions was investigated. Chapter 6 expands on the results from Chapter 5 by adjusting parameters then comparing with hydrogen data. The aim of this thesis is to show that the microtubular SOFC can be reduced and operated entirely on methane, giving great benefit to domestic consumers who do not have access to hydrogen

Chapter 2

Solid Oxide Fuel Cells

2.1 SOFC back ground

The purpose of this chapter is to review the present state of development in SOFC technology.

2.2 Actual Performance

Electrical energy is obtained from a cell when a reasonable current is drawn. However, the actual cell potential is decreased from its equilibrium potential because of irreversible losses as shown in Figure 2.1.

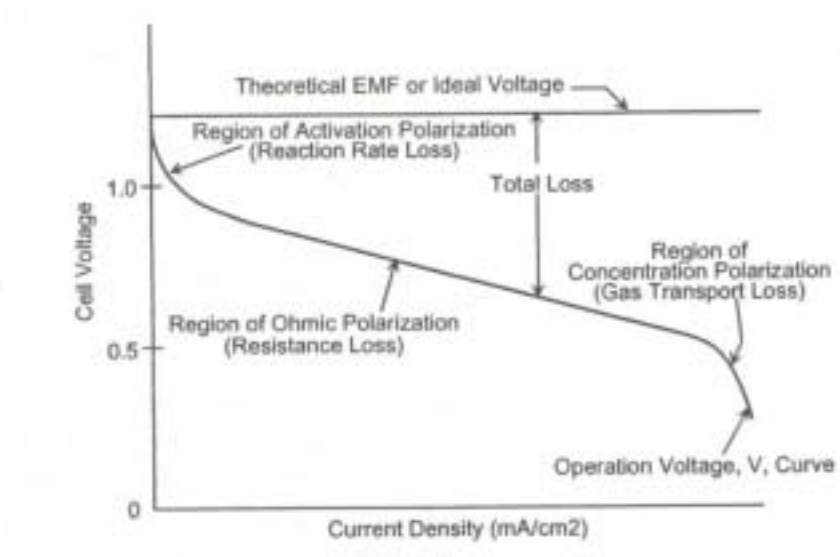

2.1 Ideal and actual fuel cell characteristic [6]

In reality, there is a deviation from the ideal behavior. The actual cell potential is

decreased from its theoretical EMF (Ideal voltage or equilibrium potential) because of irreversible losses, as shown in Figure 2.1. Several phenomena contribute to irreversible losses in the fuel cell. The losses, which are arise from polarisation, over-potential, or over-voltage, originate primarily from three sources, activation, ohmic and concentration and result in the loss of cell voltage (V) [10].

Activation polarisation: Activation polarisation is present when the rate of an electrochemical reaction at an electrode surface is controlled by sluggish electrode kinetics. In other words, activation polarisation is directly related to the rates of electrochemical reactions. There is similarity between electrochemical and chemical reactions in that both involve an activation barrier that must be overcome by the reaction species.

Ohmic polarisation: Ohmic losses occur because of resistance to the flow of ions in the electrolyte and resistance to flow of electrons through the electrode. The dominant ohmic losses through the electrolyte are reduced by decreasing the electrode separation and enhancing the ionic conductivity of the electrolyte.

Concentration polarisation: As a reactant is consumed at the electrode by

electrochemical reaction, there is a loss of potential due to the inability of the surrounding material to maintain the initial concentration of the bulk fluid. This is how a concentration gradient is formed. Several processes may contribute 1) slow diffusion in the gas phase in the electrode pores, 2) solution/dissolution of reactants/products into and out of the electrolyte, or 3) diffusion of reactants and products through the electrolyte to and from the electrochemical reaction site. At practical current densities, slow transport of reactants and products to and from the electrochemical reaction site is a major contributor to concentration polarisation.

2.3 Fuel Cell Performance Variables

The performance of fuel cells is affected by various operating parameters and other factors that influence the ideal cell potential, for example temperature, pressure, gas composition, reactant utilisation, current density, impurities and cells life. Any number of operating parameters can be selected for application of a fuel cell system, as illustrated by Figure 2.2

Figure 2.2 shows the V-I characteristic of a fuel cell in the linear range. Changing operating parameters can have either a beneficial or a detrimental impact on fuel cell performance and on the performance of the overall system. Changes in

operation conditions may lower the cost of cell, but increase the cost of the surrounding system. These parameters are based on defining specific system requirements.

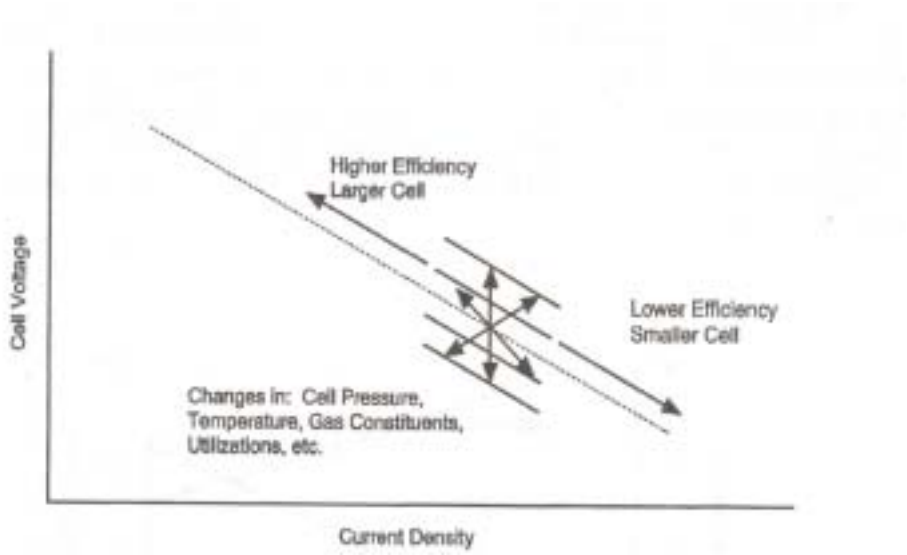

Figure 2.2 Flexibility of the cell operating parameters [6]

A design point at high current density will allow a small size at lower cost but a low efficiency results. This type of operating point would be typified by a vehicle application where light weight and small volume are required. Operating at a lower current density, but high voltage would be more suitable for stationary power plant [6].

2.4 Cell components

There are 4 key components in SOFC manufacture. The materials for different cell components have to be selected based on the following requirements [23,29].

- Suitable electrical conducting properties required of different cell components to perform their intended cell functions.
- Adequate chemical and structural stability at high temperatures.
- Minimal reactivity and inter-diffusion among different cell components
- Matching thermal expansion among different cell components.

2.4.1 Electrolyte

Solid electrolytes should satisfy numerous requirements, including: fast ionic transport, negligible electronic conduction and thermodynamic stability over a wide range of temperature and oxygen partial pressure. In addition, they must have thermal expansion compatible with that of electrodes and other construction materials, suitable mechanical properties and negligible interaction with electrode materials under operation conditions [38].

The best known oxide ion conductors have the fluorite, perovskite or pyrochlore structures. Fluorite-structured oxide materials such as yttria stabilized zirconia (YSZ) [39, 40] rare earth [41], rare earth doped ceria and rare earth doped bismuth

oxide have been studied as electrolytes for fuel cells [42-43]. Of these materials, YSZ has been most successfully employed [44].

The yttrium oxide dopant serves dual roles: it stabilizes the high temperature cubic phase in zirconia and also generates oxygen vacancies. Early zirconia based electrolytes used CaO-stabilised ZrO_2 (CSZ), but this was quickly phased out and replaced with Y_2O_3-stabilised ZrO_2 (YSZ) [45] due to higher ion conductivity and lower activation enthalpy.

YSZ forms the basis for the majority of modern SOFC electrolytes [45, 46] and has been widely studied due to its high ionic conductivity, low electronic conductivity and stability under both oxidising and reducing conditions [47-49]. Within zirconia research, there is much interest in dopants other than Y_2O_3 that may give better performance as a SOFC electrolyte. Sc_2O_3 and Yb_2O_3 in particular have been studied due to improved ionic conductivities [50, 51], though cost and long-term performance issues currently limit their effectiveness.

CeO_2 is another fluorite that has been studied due to high ionic conductivities. However, CeO_2 shows electronic conductivity at high temperatures and tends to reduce if oxygen partial pressures are low, reducing its potential as an electrolyte

material [52, 53]. Research has focused on intermediate temperature applications and suitable dopants include CaO, Y_2O_3, Gd_2O_3, Sm_2O_3 and Bi_2O_3 [54, 55].

Several electrolytes based on the perovskite (ABO_3) structure have been discovered including $LaGaO_3$ doped with group 2 or transition elements,[56-59] Ca-doped $LaAlO_3$ [60] and $LaScO_3$.[61]. Electrolytes with other structures such as $Ba_2In_2O_5$, $Sr_3In_2HfO_8$ and $Nd_{10}Si_6O_{27}$ have also been studied, but to a much lesser extent due to effective market domination by the fluorites and perovskites [62-65].

2.4.2 Anode

The anode not only serves to provide electrochemical reaction sites for oxidation of the fuel but also it allows the fuel and by products to be delivered and removed from the surface sites. An anode is supposed to exhibit sulfidation resistance and ought to be fuel flexible. Easy fabrication, and low cost are important for wide range of commercial application.

The electrical resistance of the anode is essentially composed of internal resistance, contact resistance, concentration polarization resistance and activation polarization resistance [29, 49]. Due to the requirement of high electrical conductivity, pure porous metallic electrodes in principle can be used as anodes.

Several metals such as Ni, Pt and Ru have been studied as anode material [66, 67]. The material most commonly used for SOFC anodes is a mixture comprising Ni and yttria-stabilized zirconia (YSZ) because of their low cost. It is also chemically stable in reducing atmosphere at high temperature and thermal expansion is similar to YSZ-electrolyte [29, 68, 69].

Ni and YSZ are essentially immiscible in each other and non-reactive over a very wide temperature range. The nickel phase of this anode is an excellent reforming catalyst and electrocatalyst for electro chemical oxidation of fuel. It also provides predominant electric conductivity for anode. The YSZ constitutes a framework for the dispersion and adhesion of Ni particles to the electrolyte and acts as an inhibitor for the coarsening of Ni powders [70]. It offers a part of ionic contribution to the overall conductivity, thus effectively broadening the three-phase boundaries [71].

The physical properties of both the Nickel oxide and YSZ powders have significant effects on the electro-chemical performance and fabrication process on the Ni/YSZ cermet anodes. Also average particle size, particle size distribution and sintering behaviour of both YSZ and nickel oxide powders are very important properties for the success of cell preparation [72].

Recently, several new anode materials have been investigated for direct introduction of hydrocarbons and for suppression of carbon formation during power generation such as Cu-containing anode [73], alkali earth oxide additives to Ni-YSZ anode [74], TiO_2-Based Oxides [75], CeO_2-based Oxides [76]. Also noble anode materials such as Ru-YSZ were examined to enhance the fuel flexibility of SOFC [77, 78]. Ruthenium has the advantage of a better resistance to sintering and also a higher reforming activity compared with nickel. The major disadvantage is the low availability and high cost of ruthenium oxide [78].

2.4.3 Cathode

The standard SOFC cathode material is an electronically-conductive oxide ceramic based on perovskite lanthanum strontium manganite. The high operating temperatures limit the choice of cathode materials to noble metals and electronic conducting oxides.

Requirements of cathode materials are [79]:

- High electric conductivity
- Chemical stability at operation temperature
- Chemical stability and thermal expansion closely matched to other

components

- Porous microstructure allows some oxygen transport resistance

A composite of A-site-deficient strontium-doped lanthanum manganite (LSM) and the electrolyte material, yttria-stabilized zirconia is currently used as cathode in SOFC [80, 81]. The most common cathode material is $LaMnO_3$ doped with Sr to give $La_{1-x}Sr_xMnO_{3-x/2}$ (LSM) [82, 83] and different properties can be obtained by substituting Ce, Nd, Ca, Co and Pr [1, 84, 52]. Similarly, $LaCoO_3$ can also be used as a cathode and is often doped with Sr, Ce, Dy and Fe [85-87]. Solid solutions of doped $LaMnO_3$ with $LaCoO_3$ and $LaCrO_3$ [1] have also been studied.

$LaMnO_3$ and $LaCoO_3$ are popular choices for cathode composition, however there has been progress and research into other compounds such as $Sm_{1-x}Sr_xCoO_3$ (SSC), $Pb_2Ru_2O_{6.5}$ and $La_{1-x}Sr_xCuO_{2.5-\delta}$ [88-93] as cathode materials.

2.4.4 Interconnects

Interconnects in SOFCs are the components which electronically connect the single cells. Important requirements are good electronic conductivity, gas tightness, chemical compatibility with adjacent components of fuel cell and chemical stability in reducing and oxidising atmospheres [94-95]. Usually ceramic

and metallic materials are used for the interconnect [1].

The most common ceramic interconnects of present SOFC systems are based on the perovskite structure of $LaCrO_3$ but Ca-doped $YCrO_3$ has also received some attention [96-98]. By modifying the stoichometry with other elements it is possible to adapt these interconnects with respect to thermal expansion and behaviour in the presence of reaction gases. However the principal disadvantage is low sinter ability of the interconnect material, which prevents gas tightness and low-cost production by sintering under ambient atmospheres [99, 100].

The choice of metallic interconnect is essentially governed by its corrosion characteristic. Metals are cheap and simpler to fabricate than ceramics: however, they need a drop in SOFC operating temperature. Cr-based alloys and high Cr ferritic steels enjoy most research attention, but nickel based alloys, melting pt alloys and silver steels are also studied [101-103].

2.5 SOFC Cell Configuration Options

As with the other cell types, it is necessary to stack SOFCs to increase the voltage and power being produced. Although single-cell tests provide useful information about fuel reactions and construction materials, for any SOFC to be used in a real-world application it must form part of a multi-cell stack. There are several ways of

connecting individual cells together so that they form a single unit rather like tube or plate heat exchangers [1,46].

SOFC designs have been based around two primary geometries (Tubular and Planar). The planar SOFC may be in the form of a circular disc or square plate and the tubular SOFC may be of large or small diameter

Present SOFC designs make use of thin film concepts where films of electrode, electrolyte, and interconnect material are deposited one on another and sintered, forming a cell structure. The fabrication methods differ according to the types of SOFC design. Experimental SOFCs with a planar type were evaluated in the early 1960s. However this design presented a problem for building cell stacks because it is difficult to fabricate large flat, thin cells with adequate gas sealing.

A tubular design adopted by Westinghouse and ABB for SOFCs, appeared to alleviate the problem with gas seal and thin layer surface fabrication. In this tubular design individual fuel cells were arranged in bands along the support tube and connected in series by a ceramic interconnect material [5].

2.5.1 Planar

Components of the cell are arranged in a flat orientation and are electrically connected in series. Figure 2.3 shows a typical planar configuration [1]. A similar concept with planar supports, known as the integrated planar SOFC, has recently been developed at Rolls-Royce [104].

Planar cells by their general shape tend to be more easily incorporated into flat stacks. The flat plate design in particular allows simple stacking with the shape of interconnects providing fuel and oxidant flow channels.

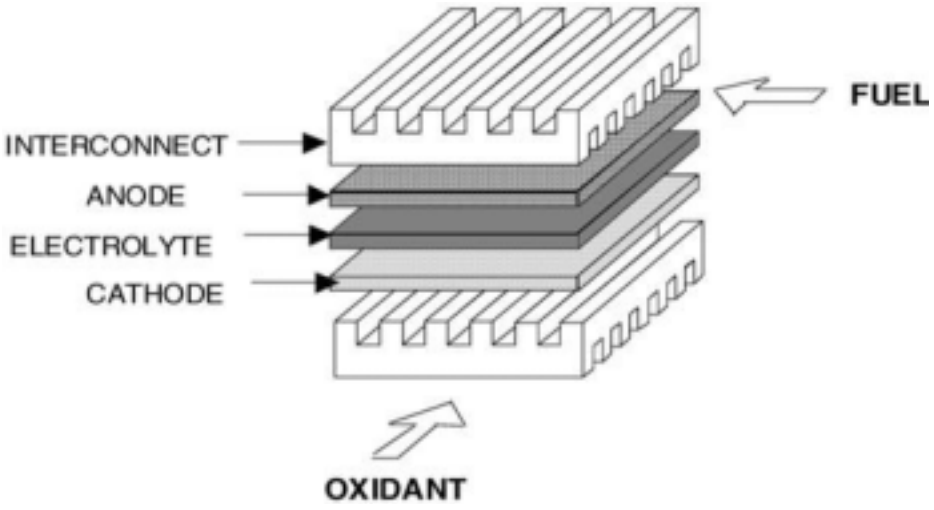

Figure 2.3 Typical planar cell with interconnects[6]

However, gas leaks in a SOFC of planar configuration with compressed seals are

difficult to prevent and thermal stress at the interface between dissimilar materials must be accommodated to prevent mechanical degradation of all cell components [10].

2.5.2 Tubular

The tubular design was developed by Siemens Westinghouse since the 1970s. Figure 2.4 schematically illustrates the design of the tubular cell [84].

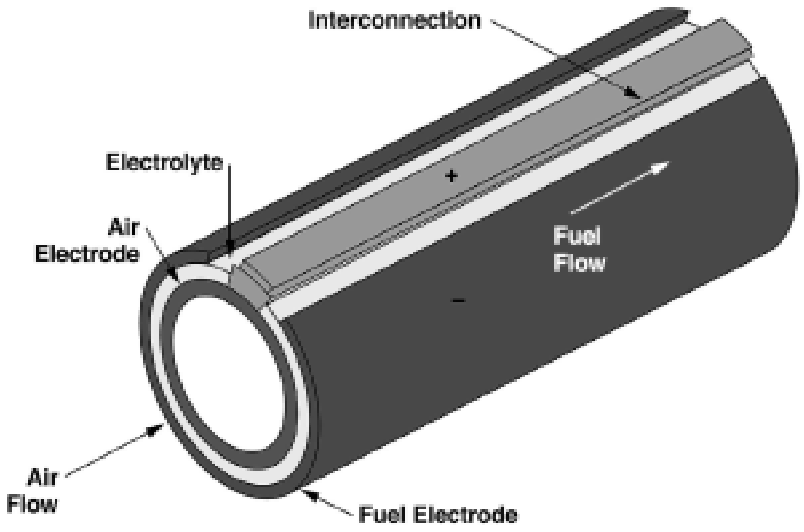

Figure 2.4 Solid Oxide Fuel Cell tubular design [105]

A major advantage of this design over earlier designs was that larger, more commercialised, systems (such as the Siemens-Westinghouse) adopted an advanced seal-less design where $LaCrO_3$ interconnects and Ni felt join adjacent anodes and cathodes, eliminating the need for high temperature gas-tight seals [1].

2.5.3 Microtubular

Microtubular solid oxide fuel cells were pioneered by Kendall in the early 1990's [106-107]. They are <4 mm in diameter and are between 50 – 100 mm in length. One of the major benefits was high thermal shock resistance [108-109]. Another major benefit of this design type was the high power density. Volumetric power density is inversely proportional to tube diameter. Consequently, the micro-tubular diameter of only 2mm in the micro-tubular design could theoretically provide up to ten times more power at the same stack volume than the previous Siemens Westinghouse design of 20mm diameter cathode supported fuel cells [10].

2.5.4 Design Requirement

Solid oxide fuel cells are manufactured in both planar and tubular form. However, there is also a sub-category, the type of support that is used. SOFCs are primarily made in three forms: electrolyte, electrode and metal supported, with electrolyte and anode supported cells being most widely used (Figure2.5).

Electrolyte supported cells are typically between 100 – 250 μm in thickness of YSZ (electrolyte). The anode and cathode are applied in layers of approximately 30 -50 μm. Advantages are a high mechanical strength and a lower susceptibility to reoxidation; however, lower electrical conductance and higher operating

temperatures are a major disadvantage.

Figure 2.5 The different types of SOFC A) Electrolyte supported fuel cell, B) Anode supported fuel cell

Anode support is the popular choice because of lower overall resistance. In the planar geometry, the anode is typically 500 μm thick and the electrolyte and cathode between 20 - 50 μm thick. It is offered by the core program of the *Solid state energy conversion alliance (SECA)* in the USA and by *Forschungszentrum Julich,* Germany.

In tubular cells the anode is between 500 μm to 3000 μm thick and for microtubular between 200 to 500 μm – dependant on length and outside diameter. The advantages are improved electrical conductance and lower operating temperature, but a disadvantage is that mechanical strength is reduced and thick electrodes lead to mass transfer problems [108, 109].

SOFCs can also be manufactured using a porous substrate as a support or using the interconnect material. The primary advantage of using these two methods is that the thin functional layers can be applied. This results in lower operating temperatures; however, cell complexity increases because the extra support material must be matched to the other four SOFC materials.

2.6 Application

SOFCs for power supplies are still under development and insufficiently advanced to have many commercial applications outside of research and development. Cost reduction will come with further refinement of materials and designs, as will the required improvements in long-term performance and stability.

SOFC systems have been developed for a wide range of devices. From portable (e.g., 500 W battery chargers), small power systems (e.g., 5 kW residential power or automobile auxiliary power units) to distributed generation power plants (e.g., 100–500 kW systems). Some examples of SOFC power system concepts are 20 W and 500 W portable power systems for use with military applications [110] for remote charging and as auxiliary power. SOFC battery hybrid vehicles [111-113] have also been studied. SOFC and other fuel cell applications are shown in Figure 2.6.

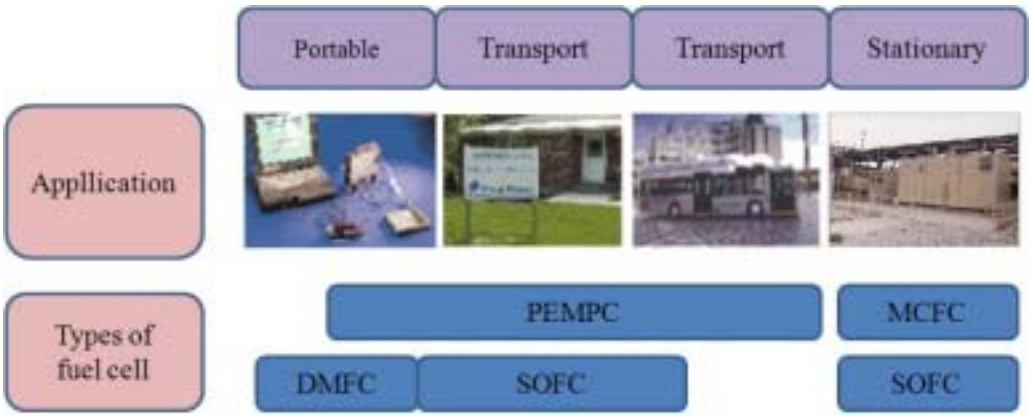

Figure 2.6 A summary of fuel cell applications [110-113]

2.7 Thermal and Redox Cycling

Thermal and Redox behaviour is an important aspect of SOFC design because the fuel cell must be switched on and off as demand varies. Stability under redox conditions is very important in Ni anode materials [114]. The problem is caused by expansion of the nickel anode being oxidized as the SOFC is subjected to transient conditions.

The main problem is the mechanical stress caused by expansion and shrinkage, which can destroy the anode structure while propagating cracks or delaminations. Other factors include increased residual stress levels, thermal shock, thermally induced stress, fatigue, coefficient of thermal expansion mismatch between the various membrane components and stress concentrations at defects. SOFC's are subject to stress in every step from manufacture to operation [115, 116]. One of

the main problems of the cell failure is residual stress. It begins to build from the fabrication process.

In the manufacturing process, the ceramics are mixed with binder and water into a slurry [117]. This is then densified, as the moisture is lost. During this process there is a significant increase in the residual stress level and the manufacturing technique can affect cracking in later stages.

Redox and thermal cycling acts in addition to the stresses created during manufacture and preparation. It can cause severe physicochemical and thermo-mechanical changes [116,118-120] in microstructure, which could lead to cracking and delamination.

When the electrolyte thickness was reduced, the redox reaction was much less damaging to the structure and electrical mechanical performance was improved. Also this problem could be eliminated if perovskite anodes were developed to replace the nickel [114] because such materials do not oxidize significantly during shutdown.

2.8 Fuelling SOFCs

Fuel cells are normally fuelled on hydrogen. However, there are several problems relating to hydrogen. One of the biggest problems is that an estimated 96% of hydrogen is produced by reforming hydrocarbons [121], and even with highly optimised large-scale production, approximately 30% of the fuel value of the hydrocarbons is lost during this process [122]. Thus research has moved towards using alternative readily available fuels directly.

In previous papers, the SOFC operating temperature and the nickel anode afford direct internal reforming of available fuels such as bio gas, bio diesel, jet fuel and hydrocarbons [123-124].

In particular, hydrocarbon (HC) such as liquid petroleum gas or natural gas are expected in the near future to be suitable fuels which benefit from lower cost and lower pressure for storage. However, the main problem of running hydrocarbons directly into SOFC anodes is severe carbon deposition on the surface of the catalyst. This is known to lead to a decrease in cell performance resulting from the deactivation of electrocatalytic area for fuel oxidation [37].

In recent times, there has been increasing interest in the direct operation of solid

oxide fuel cells (SOFCs) on methane because natural gas is a widely available fuel. Also, bio-methane is likely to be more available in the next decades. Short chain hydrocarbon (HC) fuels have advantages for SOFCs because internal reforming on the nickel anode is possible, although generally some pre-reforming is used in practice. This reduces running cost and helps to achieve higher working efficiencies [4].

In this thesis available hydrocarbons are considered, especially methane. Pure methane was investigated to carry out the whole SOFC process from reduction to operation.

2.8.1 Fuel Reforming

The basic fuel cell reactions are the oxidation of hydrogen to water, the oxidation of carbon monoxide to carbon dioxide and the direct oxidation of hydrocarbons, as shown below.

$2H_2 + O_2 \rightarrow H_2O$

$2CO + O_2 \rightarrow 2CO_2$

$CH_4 + 2O_2 \rightarrow 2H_2O + CO_2$

Instead of direct oxidation, fuels can be reacted with an oxidising agent: The most common methods being steam reforming, partial oxidation and dry reforming [37, 124-128]. Steam and dry reforming are endothermic, while partial oxidation is exothermic. These reactions can be used to convert methane into a gas mixture of hydrogen and carbon monoxide, which potentially leads to less carbon deposition on the anode.

$CH_4 + H_2O \rightarrow 3H_2 + CO$	Steam reforming
$CH_4 + ½O_2 \rightarrow 2H_2 + CO$	Partial oxidation
$CH_4 + CO_2 \rightarrow 2H_2 + 2CO$	Dry reforming

During fuel cell operation, there are other competing reactions between the available gases. The most common are the water gas shift reaction and the Boudouard reaction to form carbon on the anode. Carbon can also be formed through hydrocarbon pyrolysis, and removed through steam gasification.

$H_2O + CO \leftrightarrow H_2 + CO_2$	Water gas shift
$2CO \rightarrow C + CO_2$	Boudouard reaction
$CH_4 \rightarrow C + 2H_2$	Pyrolysis
$C + H_2O \rightarrow CO + H_2$	Stream gasification

Reforming enables SOFC to use hydrocarbon directly as fuel. There are two methods which have been developed, external and internal reforming. In external reforming, the reaction occurs in a separator reactor, which consists of heated cells filled with nickel or noble metal. In internal, natural gas reforming can be directly carried out at the anode of the fuel cell. Advantages of internal reforming are the good and direct heat transfer between stack and reforming zone and high degree of chemical integration. Other advantages include reduced system cost and higher methane conversion rate. [23]

Methane is a strong candidate fuel for SOFC applications [129-133]. However, the details of methane reactions during anode reduction have received surprisingly little attention considering that it is the principal component of natural gas.

2.8.2 Carbon Deposition and Poisoning

Although the high operating temperature and metallic anode of the SOFC make it suitable for the direct reforming of hydrocarbons the main problem is carbon deposition [3-4]. Hydrocarbons can be oxidised on the anode to produce some electrical power, but as a consequence, they also produce several unwanted carbon coking reactions. For example, nickel is well known for its propensity to promote

hydrocarbon pyrolysis and hence cause carbon to deposit [135].

This deposition leads to the deactivation of catalyst sites and, in extreme cases, physical blockage or fracture of the cell. It is avoided by judicious choice of reaction conditions (e.g. temperatures too low for carbon to form) or by the addition of an oxidant (typically water) to oxidize deposited carbon to CO_2. A C:O ratio of at least 1 is usually required to avoid carbon build-up, and carbon-free conditions may necessitate a ratio of up to 8.

Thermo dynamic equilibrium calculations provide a first approximation of potential for coke formation. Indications at what conditions carbon may be formed for hydrocarbon fuels are determined by the simultaneous solution of the above equations using their equilibrium coefficients. No solid graphitic carbon exists at low temperatures in binary mixture containing at least 2 atoms of oxygen or 4 atoms of hydrogen per atom of carbon [134].

Some new materials were proposed to decrease the catalytic activity of Ni for reforming, in order to avoid carbon deposition without using excess steam (for example, doping with Mo, Cu, Ru or Au)[135-136]. The iron achieves a decrease in a catalytic activity of nickel and adjusts the thermal expansion coefficient

closer to YSZ. The approach of optimising the methane itself, other than through reforming reactions, has not been extensively studied and is thus the principal objective of this investigation.

Fuel cell electrodes like all other catalyst are easily poisoned. When using gas, the key poison is sulphur, hence this is typically removed using a de-sulphuriser. Metal catalysts in the fuel reformer can be susceptible to sulphur poisoning and it is very important that sulphur in the fuel reformate be removed. There are high and low temperature methods to remove sulphur from a fuel reformate stream. Low temperature clean up, such as hydro desulfurizing, is less difficult and lower in cost so should be used where possible, certainly with low temperature [10].

2.8.3 Performance Degradation

Degradation problems in long term operation of SOFCs are characterized by a gradual decrease in performance of the fuel cell. The most probable reason for performance degradation in hydrogen is Ni agglomeration [137], which takes place during long term testing.

Lowering the melting temperature of Ni by alloying additions caused increased

sintering close to the SOFC operating temperature. This sintering of Ni anodes in a reducing environment can be very rapid and form many isolated melted pools of nickel metal [138].

Over long periods of testing, the average Ni particle size increased from 2μm to almost 3μm as additional electronic Ni-to-Ni contacts formed [139]. The microstructure changed with agglomeration and it coarsened in the Ni phase and formed nickel hydroxide, both of which can contribute to fuel cell degradation. Degradation in hydrocarbon fuels is largely associated with carbon deposition [140]. This can happen much more rapidly than the Ni aggregation, in a period of minutes.

2.9 Conclusion

In this chapter SOFC technology has been introduced. The conclusion of the literature review was that several different designs are available each with their own benefits. Because small tubular cells are so advantageous in terms of power density and transient performance, this thesis is to be based on the micro-tubular technology.

The design is to be Ni/YSZ anode supported with a LSM cathode, and 8% YSZ

electrolyte. In the following chapters the objective is to test carbon deposition in a micro-tubular SOFC and to find optimum conditions of reduction and operation which would inhibit the carbon damage problem at the anode.

Chapter 3

Materials and Methods

3.1 Overview

The purpose of this chapter is to describe the materials and the experimental set-up for investigating the anode-supported micro tubular fuel cell.

3.2 Preparation of Anode Supported Microtubular Fuel Cells

3.2.1 Anode and Electrolyte

Figure 3.1 shows an anode support raw material tube. These tubes were based on 5 cm long extruded anode supported YSZ tubes of 2.5 mm outside diameter with a wall thickness of approximately 0.5 mm (supplied by Adaptive Materials Inc. USA.)

Figure 3.1 Pre-fired NiO/YSZ tube supplied by Adaptive Materials Inc.

3.2.2 Cathode

As shown in table 3.1, the cathode electrochemical layer was applied using an LSM/ZrO_2 ink; 6.5g $La_{0.5}Sr_{0.5}MnO_3$ (Seattle Speciality Ceramics), 6.5g YSZ

(Tosoh TZ8Y), 16g acetone, 0.25g KD2 surfactant and 0.2g glycerol trioleate milled for 24 hr using zirconia beads to form an ink which was painted on the outside of the electrolyte tube. A second layer was applied using 20g LSM (Merck $La_{0.82}Sr_{0.18}MnO_3$), 0.2g KD2, and 14g acetone.

	Materials	Maker	Grade	Wt%
Cathode 1	LSM [1)]	Seattle Speciality Ceramics	$La_{0.5}Sr_{0.5}MnO_3$	6.5g
	YSZ [2)]	TOSOH	TZ8Y	6.5g
	KD2 [3)]	ICI	-[4)]	0.25 g
	Glycerol Trioleate	Aldrich	A.C.S reagent	0.2 g
	Acetone	Aldrich	A.C.S reagent	16 g
Cathode 2	LSM	Merck	$LA_{0.82}Sr_{0.18}MnO_3$	20 g
	KD2	ICI	-[4)]	0.4 g
	Acetone	Aldrich	A.C.S reagent	14 g
	Terpinol	Aldrich	A.C.S. reagent	2 g

1) Lanthanum strontium manganite 2) yttria stabilized zirconia 3) polyoxyalkylene amine derivative
4) Sodium chloride, polyethylene glycol and water mixture.

Table.3.1 Materials for the preparation of tubular cell cathode

Figure 3.2 Cathode sintering profile

Once the ink was manufactured it had to be applied to the outer surface of the raw micro tube. This was achieved by painting. Cathode layer 1 was applied to a length of 30 mm and left to dry overnight. Following this, cathode layer 2 was applied over layer 1.

This was left to dry for 2 hours before sintering. The cathode layers were then sintered inside a Carbolite^{TM} furnace on a programmed profile given in Figure 3.2, the sintering peak temperature being 1150 ^{o}C.

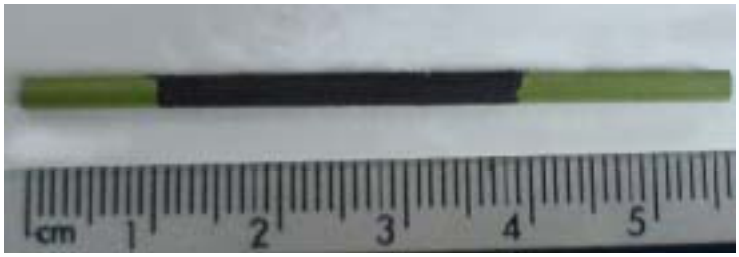

Figure 3.3 NiO/YSZ tube with two layers of LSM sintered cathode

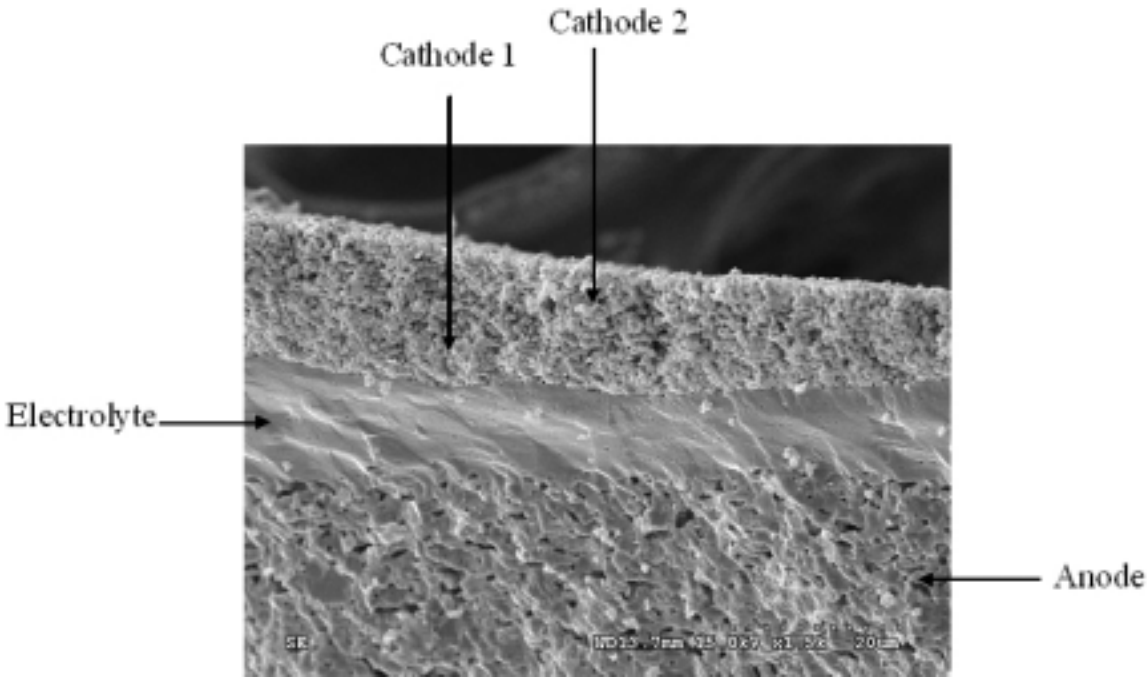

Figure 3.4 Field Emission Scanning Electron Microscope (FE-SEM) image of cross section of the micro tubular SOFC

Figure 3.3 shows the fuel cell at this stage. The cathode was painted off centre to allow space for the fuel injector. Using a Hitachi S-4300 Field Emission Scanning Electron Microscope (FE-SEM), the tubes were examined (Figure 3.4). From the images, the thickness of the cathode was measured to be about 50㎛.

3.2.3 Fuels

Fuel gases were supplied by British oxygen Company (BOC) UK as follows:

●Helium 99.99%

●Hydrogen 99.95%

●Methane CP Grade 99.95%

3.2.4 Reduction

After sintering the cathode, the tubes were reduced in either hydrogen or pure methane. The reduction process was completed by packing 5 tubes inside a quartz glass reactor. Three different types of reduction experiments were examined, varing fuel flow rate, temperature and time. The cell with 2 layer cathodes after reduction is illustrated in Figure 3.5.

Figure 3.5 NiO/YSZ tube with two layers of LSM sintered cathode after reduction

3.2.5 Interconnects

After reduction, 3 silver ink bands 2 mm in width for current collection were painted onto the cathode, spaced equally along the length. They were linked together with a silver ink line. 50 mm of 0.25 mm diameter silver wire (99.99% Goodfellow) was then used for cathode current collection, wound over the silver bands. Figure 3.6 shows the complete cathode connection.

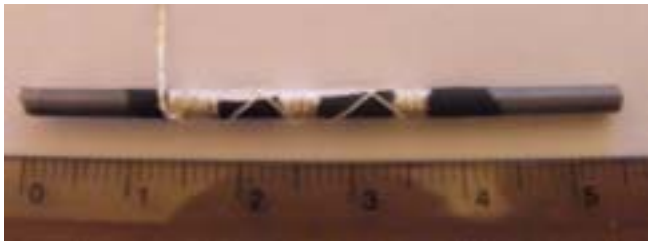

Figure 3.6 A SOFC with silver in bands and wire

3.2.6 Internal Mesh and Pin

To make the anode current collector, The mesh and pin technique method has been widely employed by previous researchers [4, 141-148] in manufacture of micro tubular cells. Figure 3.7 shows a rolled mesh and a complete fuel cell. A nickel mesh (DexMet Microgrid) was cut and rolled to the correct length (55 mm) and diameter (2mm). As nickel metal has a much higher specific electrical conductivity than Ni/YSZ anode, a nickel mesh was inserted into the fuel cell to act as an anode current collector. This mesh was held in place with a sized nickel

pin which provided an additional conduction.

The length of the mesh was 50 mm; this enabled a small amount to extend past the end of the tube, hence enabling an interconnection to be made. The 2 mm diameter enabled commensurate contact between the nickel mesh and the anode surface.

A)

B)

Figure 3.7 shows a rolled mesh and pin (A) and a completed fuel cell (B).

A nickel pin (Micro Metallic) of width 2 mm was added and silver wire was wound onto the end of the nickel mesh. This ensured that contact was maintained with the anode surface inside the tube.

3.3 SOFC testing and analysis

The objective of the experiments was to test the tubular SOFCs on hydrogen and pure methane. For optimisation of hydrogen and methane the tubes were prepared under various conditions.

3.3.1 Reduction condition of SOFC

Temperature: The tubes were reduced at constant temperature, changing the temperature for different batches from 650 ^{o}C to 850^{o}C at 50^{o}C intervals. After reduction, the cells were tested at various operating temperatures, varying the flow rate and time during the different tests.

Flow rate: 20 ml/min H_2 and various CH_4 (5 – 20ml/min) were supplied to the tubes and the tube performance was then tested to find the optimum conditions.

Time: the tubes were exposed to H_2 (30 – 120 min) and CH_4 (15 – 60min) then were tested at optimum condition.

3.3.2 Test Rig

To conduct the experiment, the tubular cell was inserted into the experimental furnace as shown in figure 3.8. The fuels were supplied from cylinders, then

metered by 3 X Unit Instrument 7300 mass flow controllers, mixed and then passed through to the fuel cell. A university built potentiostat was used to withdraw power from the system. The power withdrawn was controlled using a purpose built program in LabView™

A MKS minilab mass spectrometer carried out gas analysis of the reformate and exhaust gases from the fuel cell. Fuel gases were not pre-heated nor humidified during these experiments. All pre-heating was conducted within the delivery tube in the furnace.

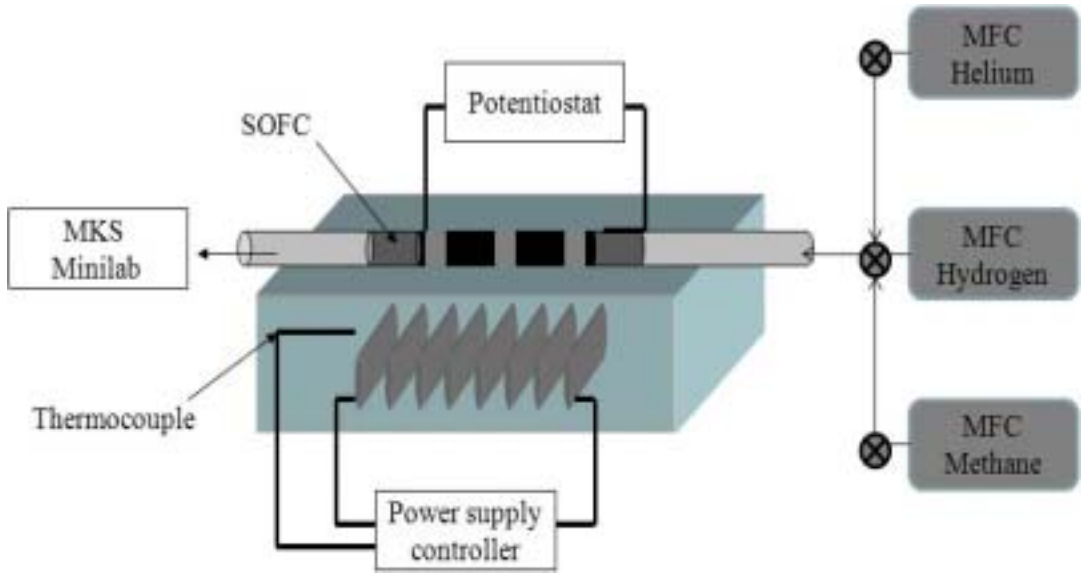

Figure 3.8 Experimental set-up for SOFC

3.3.3 Operating Condition of SOFC

Temperature: From 650 to 850^{o}C, the cells were tested at reduction optimum condition (H_2: 850^{o}C, 2hr, 20ml/min flow rate, CH_4: 650^{o}C, 30min, 10ml/min flow rate). The cells were raised from ambient to the test target temperature then tested at 850^{o}C, 20ml/min for hydrogen and 850 ^{o}C, 10ml/min for methane.

Flow rate: H_2 (5 - 20ml/min) and CH_4 (5 – 20ml/min) were supplied to the tubes then tested at 850 ^{o}C with optimum reduction condition.

Time: The tubes were tested for 500 min with optimised reduction and operation condition. (H2: Reduction at 850 ^{o}C, 2hr, 20ml/min, operating at 850 ^{o}C, operating at 850 ^{o}C, 20ml/min)(CH_4: Reduction at 650, 10ml/min, 30min, operating: at 850 ^{o}C, 10ml/min)

3.3.4 The Mass Spectrometer

The MKS Mini-Lab mass spectrometer was used to analyse the reaction products from the anode and to measure the carbon deposited during the tests. It utilises an electron ion source, quadrupole mass filter and Faraday cup detector.

In electron ionisation (EI), electrons are produced by electrically heating a wire

filament. These electrons are then accelerated towards an anode with typical energy of 70 eV. The electrons interact with incoming gas molecules on the way, causing ionisation and fragmentation.

Ionised and fragmented molecules pass through the ionisation chamber and enter the quadrapole mass filter. This consists of four parallel rods with a DC potential applied in such a way that diagonally opposite rods have the same potential. A radio frequency AC potential is also applied to the rod pairs, and incoming ions travel down the centre of the quadrapole between the rods. For a given DC and AC voltage, only ions of a specific mass/charge ratio will pass through the quadrapole; others will have unstable oscillations and collide with a rod. A mass spectrum can be obtained by varying the voltages to detect ions across a range of mass-to-charge ratios.

Ions that pass through the mass filter are detected using a Faraday cup. This is a metal cup that becomes charged when ions collide with it, and is then discharged to give a small current equivalent to the charge on the captured ions.

The mass of each ion detected is related to the size of the magnetic field used in the detector. A change in the amount of a single component affects the partial

pressure measurement of all the other components in the sample gas stream. Therefore, it is required that the mass spectrometer be calibrated with known gases such as helium or argon. More information of calibration mathematics can be found in Dhir [149] and Preece [150]

3.3.5 Calibration Mathematics

In order to determine the actual gas composition, it is necessary to perform a series of calibration experiments for the relevant gases. These gases are mixed with a known, constant flow of an inert gas (such as helium or argon) so that measurements can be made relative to this reference. Then partial pressure measurements can be converted into actual fractions or normalised against the reference gas to give absolute amounts.

Let ν_k be the correction factor for a gas component k whose mass spec. signal is given by m_k and which exists in a mixture of gases as a (percentage) fraction G_k

The corrected mass spec. signal is $m_k\,[c]$ i.e.

$$m_k\,[c] = \nu_k \; m_k$$

where:

$$\nu_k = \frac{G_k}{[m_k]^{cal}}$$

where $[m_k]^{cal}$ is the mass spectrometer signal for a known gas fraction component *k*.

If this component *k* exists with many other mass components, the percentage of component *k*, $G_k\,[c]$, is expressed as follows:

$$G_k[c] = \frac{m_k[c]}{\sum_i m_i[c]} = \frac{m_k.\nu_k}{\sum_i m_i.\nu_i}$$

Define one mass component m_r to be the mass component. Helium is used in this system. All other mass signals are measured relative to this mass.

$$G_k[c] = \frac{m_k.\nu_k}{\sum_{i \neq r} m_i.\nu_i + m_r.\nu_r}$$

Factoring the denominator bottom by ν_r

$$G_k[c] = \frac{\nu_k}{\nu_r} \frac{m_k}{\left(m_r + \sum_{i \neq r} m_i . \nu_i / \nu_r \right)}$$

And hence a definition of a calibration factor :

$$\kappa_i^r = \frac{\nu_i}{\nu_r} = \frac{G_i}{[m_i]^{cal}} \cdot \frac{[m_r]^{cal}}{G_r}$$

Hence

$$G_k[c] = \frac{m_k \kappa_k^r}{m_r + \sum_{i \neq r} m_i . \kappa_i^r}$$

In a gas mixture containing He, H_2, CH_4, CO and CO_2 the corrected gas fraction of CH_4 is :

$$G_{CH_4}[c] = \frac{m_{CH_4} \kappa_{CH_4}^{He}}{m_{He} + m_{H_2} . \kappa_{H_2}^{He} + m_{CH_4} . \kappa_{CH_4}^{He} + m_{CO_2} . \kappa_{CO_2}^{He} + m_{CO} . \kappa_{CO}^{He}}$$

If a gas mixture does not contain the reference gas, it is possible to use a different component *s* in the gas mixture as the reference without the need to re-obtain the calibration factors. The factors are related as follows:

$$\kappa_i^s = \frac{\kappa_i^r}{\kappa_s^r} = \frac{\nu_i}{\nu_r}\frac{\nu_r}{\nu_s}$$

3.3.6 Temperature Programmed Oxidation (TPO)

The total carbon deposition on the anode of the fuel cell reaction was measured calculated using temperature programmed surface oxidation. Used cells were stripped of silver wire, Ni mesh and pin, then packed into a quartz glass tube, which replaced the fuel cell in the experimental rig shown in Figure 3.8.

Helium (20 ml/min) and oxygen (2 ml/min) was supplied to the quartz tube, and the furnace was heated to 800°C at a rate of 10 °C/min. At room temperature, carbon is stable in an oxidising atmosphere. As the temperature is increased, however, different types of carbon will react to form CO or CO_2 at different times. Amorphous carbon tends to oxidise around 300°C, whereas graphitic carbon oxidizes around 600°C [124]. CO and CO_2 levels were monitored by an on-line mass spectrometer and plotted against temperature, and thus time.

Figure 3.9 showed the total carbon deposition from methane. While the calibration experiments produced similar amounts of CO and CO_2, most fuel cell experiments gave far more CO_2 than CO. This is due to the partial pressure of

oxygen and the way that carbon is laid down on nickel anodes. When CO is formed, further oxidation to CO_2 is rapid unless another nearby carbon atom can be oxidised instead.

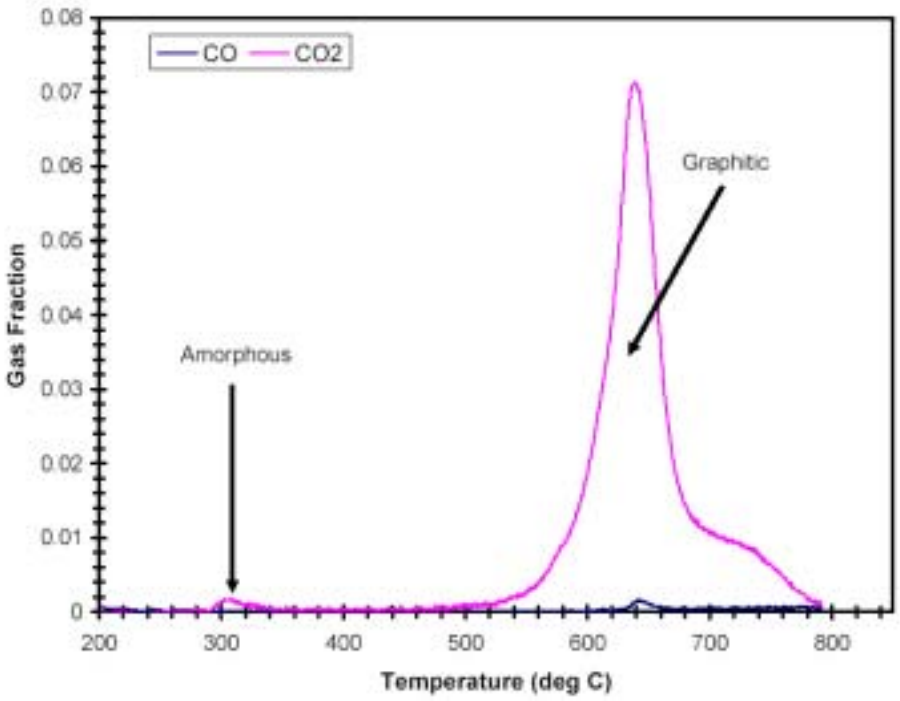

Figure 3.9 Typical TPO profile of a cell operated on methane

With a SOFC anode, there is effectively a C-Ni chemical bond, which can be oxidised to give a Ni-C-O structure. Clearly this is not present in pure carbon or carbon that is bonded to other C atoms instead of Ni -hence significant amounts of CO are only seen when there is extensive carbon deposition. The absolute mass of carbon deposited on the anode was measured then related to the amount of carbon in the fuel flowing through the cell.

The amount of carbon entering the cell was calculated from the physical properties of the fuel mix and the time and rate of addition. In this thesis, only methane reduction and operation were studied. The amount of carbon deposited was found to be also dependent on the operational condition of the fuel cell, eg temperature, as well as the composition of fuel.

3.3.7 Measurement of mechanical strength

To determine fuel cell mechanical properties, three point bending tests were performed. A universal testing machine (UTM, Instron Co., Model 4469, 500N load cell) with crosshead speed 1mm/min was used to load each tube until fracture occurred.

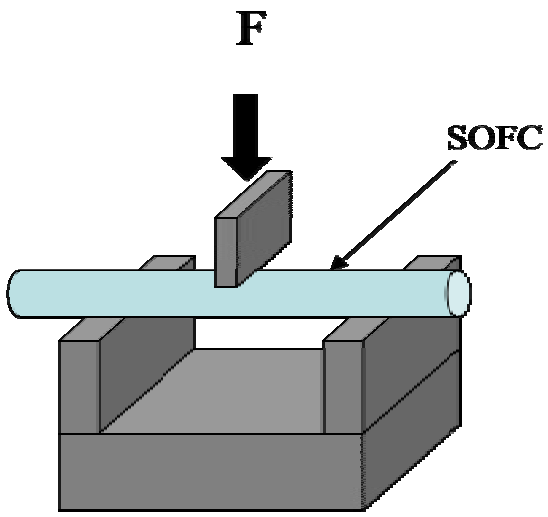

Figure. 3.10 The scheme of three point bending test measurement

The specimens were tested in non-machined condition. Figure 3.10 presents the schematic diagram of testing measurement. The maximum load was measured by pressing the centre of the specimen until fracture occurred. The dimensions of the tube cell were measured. The equation for bend strengths of a tube is

$$S = FL / \pi D_0(D_2^2-D_1^2)$$

Where, F is the maximum load, L is the distance between support, D_0, D_1,-D_2 are the mean, inner and outer diameter, respectively

It may be seen that the strength of identical tubes is proportional to the maximum bending force. Therefore, this breaking force was used to relate the relative strengths of tubes reduced in different condition.

3.3.8 Field Emission Scanning Electron Microscope (FE-SEM) and Energy-Dispersive X-ray spectroscopy (EDX)

Scanning electron microscopy was used to characterise the microstructural changes that occured after methane reduction. All SEM images were taken using a Hitachi S-4300 Field Emission Scanning Electron Microscope (FE-SEM) operating at 15 kV with a Horiba EX-200 Energy-Dispersive X-ray spectroscopy (EDX) spectrometer. Methane reduced samples were investigated to identify Ni, YSZ and carbon deposition and anode microstructures were subsequently

measured.

Chapter 4

Optimisation Condition for Tubular Cell on Hydrogen

4.1 Overview

This chapter reports the testing of optimisation conditions for anode-supported micro tubular SOFCs on hydrogen. The objective of the experiments was to test the tubular SOFCs at various hydrogen flow rates and temperatures. This was to form the baseline for comparison with later experiments on methane described in chapter 5.

4.2 Experimental

Five cells were inserted into a 15mm diameter silica tube placed in a furnace and various flows of hydrogen were injected into the tube at several temperatures. 5 reduction conditions were studied at 20 ml/min hydrogen flow; 650, 700, 750, 800 and 850^{o}C. Each condition was observed at five times; 15, 30, 45 and 60 min. The electrical testing output was recorded and the flexural strength of the SOFC microtubes was investigated. Microstructures were imaged by SEM.

Electrochemical performance of the reduced cells was tested in a 20 min period using the experimental set-up shown in Figure 3.8. An electrically heated furnace was controlled by a thermocouple and Eurotherm system. The hydrogen gas was delivered from cylinders, metered by mass flow controller and passed to the fuel cell. The electrical output at 850^{o}C was monitored by a potentiostat.

4.3 Three Point Bending Test

Mechanical strength values were found to increase with increasing reduction time as illustrated by the result in Figure 4.1, showing the time dependent breaking force data.

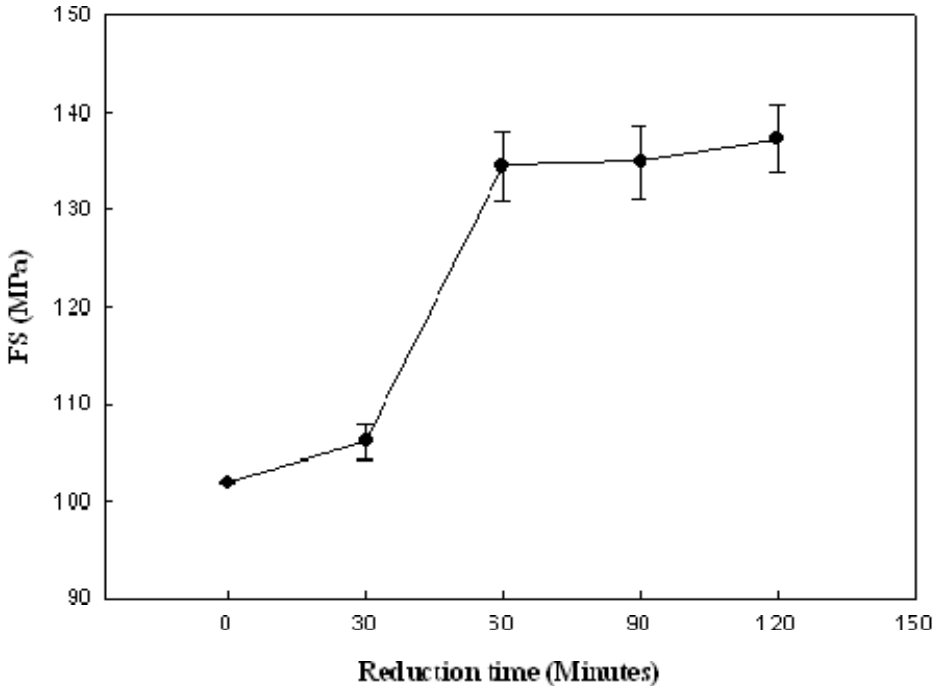

Figure 4.1 Mechanical strength of fuel cell with different reduction time on hydrogen at 750 ^{o}C

Strength values were considerably increased after 60 minutes. When hydrogen fuel was supplied to the cell for the first time, NiO-YSZ was converted into Ni-YSZ cermet. As NiO reduced to Ni-metal the volume and porosity of the anode layer was changed by the ensuing shrinkage of the NiO particles.

The strength of Ni-YSZ with the same NiO-YSZ porosity is higher because of the presence of ductile Ni-metal phase which sinters in interparticle contact. In most cases, YSZ agglomerates, also the clusters of Ni or NiO grains, as well as surface dimples are identified as a strength controlling defects [151]. Between 60 min to 120 min reduction time, there was no significant strength increase of the SOFCs though there was a slight increase in the error bars. The conclusion was that, to increase mechanical properties, SOFCs needed at least 1 hr reduction time at 750 ºC.

4.4 Influence of Reduction Time on Current output

Figure 4.2 shows the results obtained by running the SOFC on hydrogen 20ml/min at different reduction times: the temperature remained constant at 750ºC. As the reduction time increased, current output also increased. The peak current at 0.5V was approximately 1.15 A/cm^2 and the cell performed steadily as indicated by the Figure 4.2 corresponding to different flow rates of hydrogen. Again this is consistent with sintering of the Ni particles to improve current linkage.

It can be seen in the figure that performance increased as reduction time was raised. Between 1 hr and 2hr reduction, the current output was increased by 48%.

The highest current performance occurred after 2 hr reduction. It seemed that NiO particles were fully reduced to Ni particles for current output. The conclusion was that at least 2hr reduction time was needed for higher electrical performance at 750ºC. Thus, from the above results, 2hr reduction time is the best condition for electrical performance of SOFCs at 750 ºC reduction and 20 ml/min hydrogen.

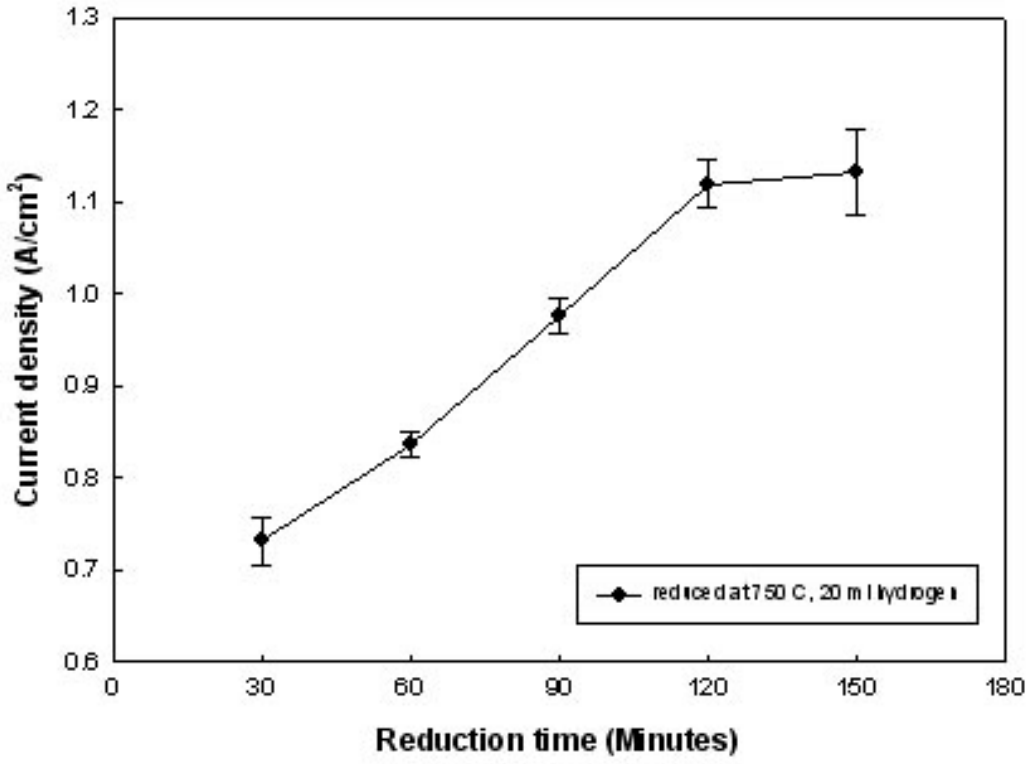

Figure 4.2 Current density vs. Reduction time at 750 ºC, 20 ml/min hydrogen, 0.5 V

4.5 Influence of Reduction Temperature

The effect of reduction on electrical performance is also seen from the current

output in Figure 4.3. This was taken during the test after 750, 800, 850, 900, 1050 ºC reduction temperature by 20 ml/min hydrogen. In these results, the slope of the V-I curve changes with time.

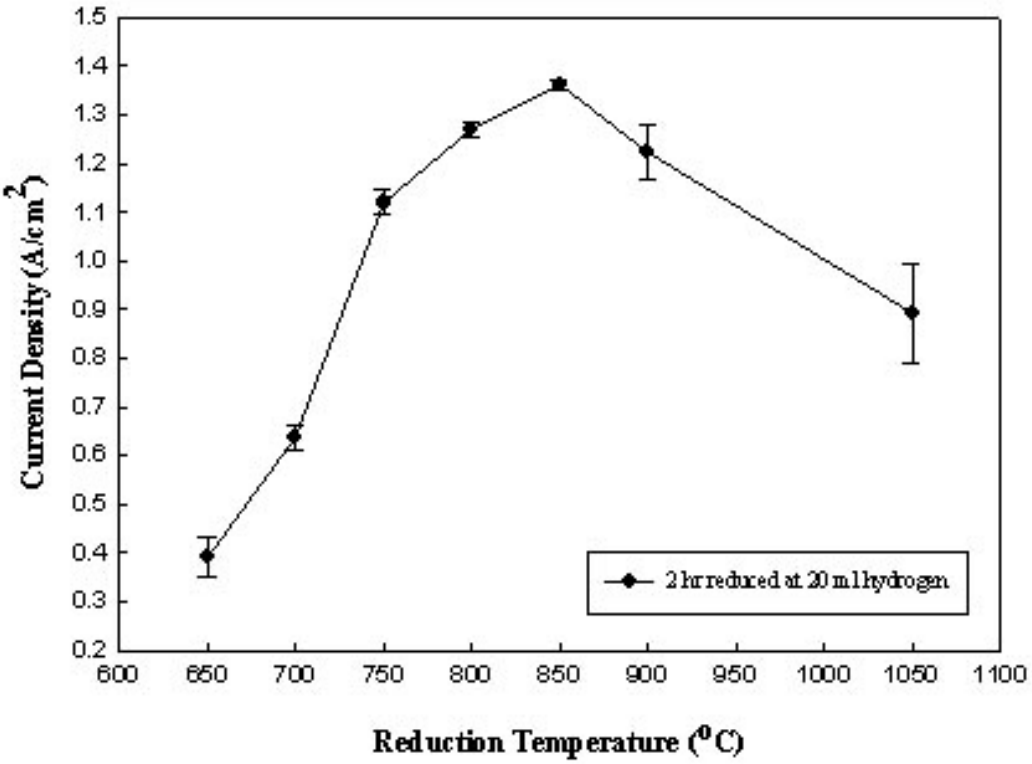

Figure 4.3 Current density for different reduction temperature, 0.5 V

The current density was significantly increased up to 850ºC reduction temperature. A performance drop occurred after the 900ºC reduction temperature because the surface of the LSM started to crack. The crack formation started over 900ºC reduction stage and the cracks further developed so that the values of current output considerably dropped because the cathode was exposed at high temperature in short time. Moreover, the electrolyte on the surface of the cell

was becoming dark over 850ºC. It seemed that the cells were damaged from over 900ºC because the LSM was diffusing into the electrolyte.

As a result, when reduction temperature were over 900ºC, the LSM cathode and the other cell components were not generating electrical properties properly. This effect may be an indication that the 2hr reduction time at 850ºC was optimal.

Scanning Electron Microscopy (SEM) was used to characterize the microstructural change that occurred during reduction at the various temperatures (Figure 4.4, 4.5). The YSZ phase started with a grain size less than 1 μm in size. Ni particles appear several microns in size.

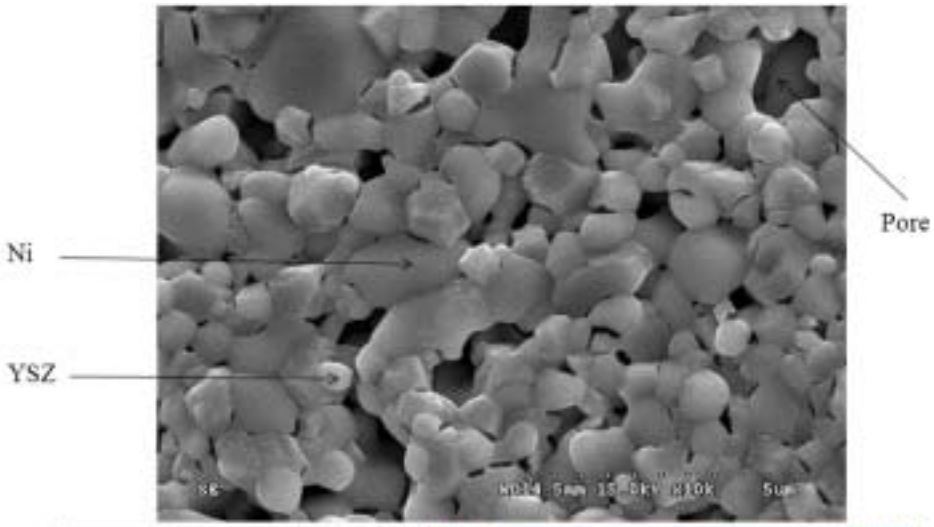

Element	Weight %	Atomic %
O	13.56	40.75
Ni	46.64	38.19
Y	6.60	3.57
Zr	33.19	17.49
Total	100.00	

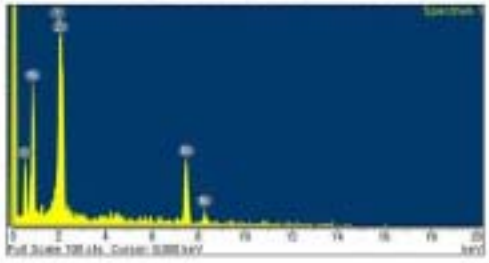

Figure 4.4 SEM image of anode after hydrogen reduction at 650 ºC, 20 ml/min, 2hr

Areas of porosity are black in the image. In hydrogen reduction the most prominent structural changes take place in localised areas. The dark gray regions belonged to clusters of Ni metal particles and the light ones were YSZ particles.

Figure 4.4 shows the anode surface after low temperature reduction. At low temperature (650ºC), small Ni particles were separate on the anode surface and it seemed that the separation of these grains was giving low electric connectivity in the anode, leading to low current. This is to be expected because nickel oxide reduces to smaller, separated, particles at low temperature, producing better catalyst properties but decreased electrical performances

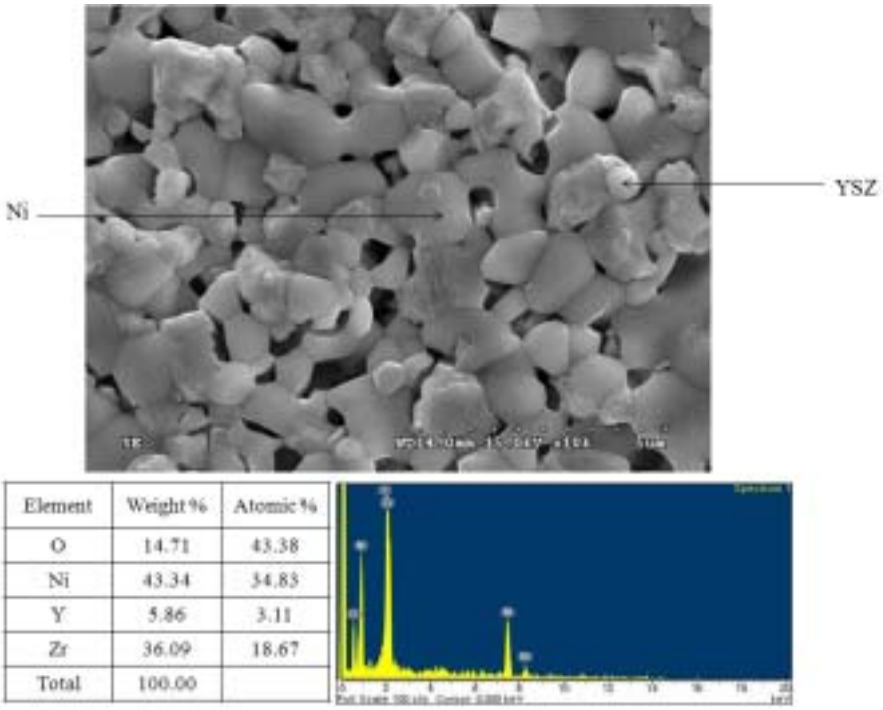

Element	Weight %	Atomic %
O	14.71	43.38
Ni	43.34	34.83
Y	5.86	3.11
Zr	36.09	18.67
Total	100.00	

Figure 4.5 SEM image of anode after hydrogen reduction at 850 ºC, 20 ml/min, 2hr

Figure 4.5 shows the anode structure after high temperature reduction, with the larger nickel particles on the surface of the porous cermet anode being well connected and giving a low electronic resistance.

4.6 Influence of Running Flow Rate

Experiments were carried out to relate flow rate and cell performance. Cells were supplied with various flow rates of hydrogen from 5ml/min to 25 ml/min between 60 and 120 min reduction time. Current values were recorded at 0.5 V.

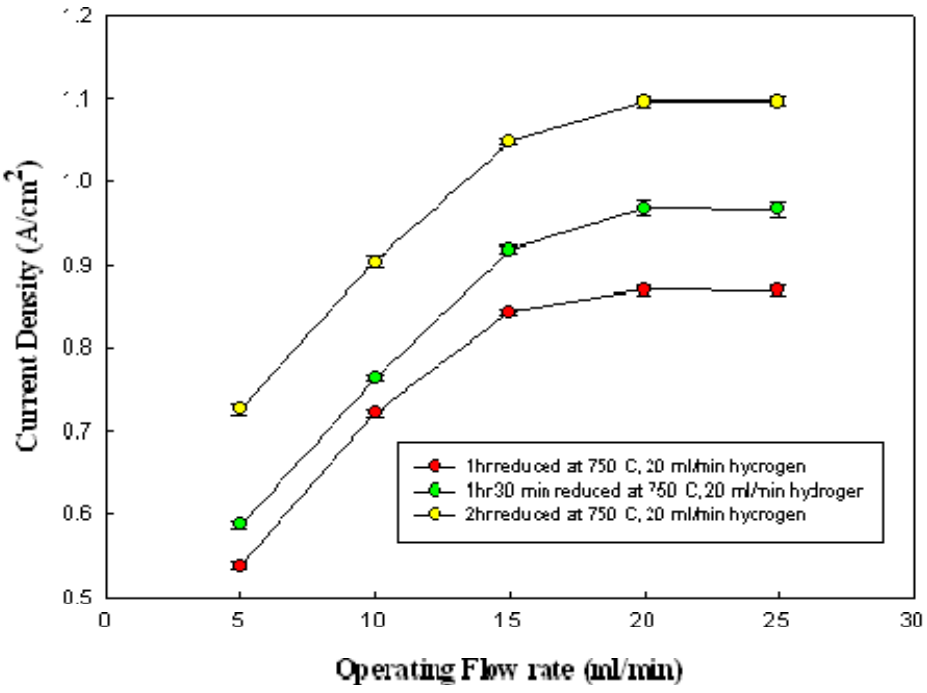

Figure 4.6 Effect of different reduction time on current density vs. time of SOFC testing different hydrogen flow rate at 750 °C, 20ml/min hydrogen, 0.5V

Figure 4.6 showed that 20ml running flow rate gave the best current output at 1.12 A/cm^2. Over 20ml/min operating flow rate, the cell performed steadily.

Also figure 4.6 showed the comparison of reduction time dependent current output. Between 1 hr and 2hr reduction current output was increased by 32%. Also these results showed that if reduction time was raised from 60 to 120 min there was an increase in current density of 26% at 20 ml/min hydrogen flow rate. Over 20ml/min there were no significant current change data not shown.

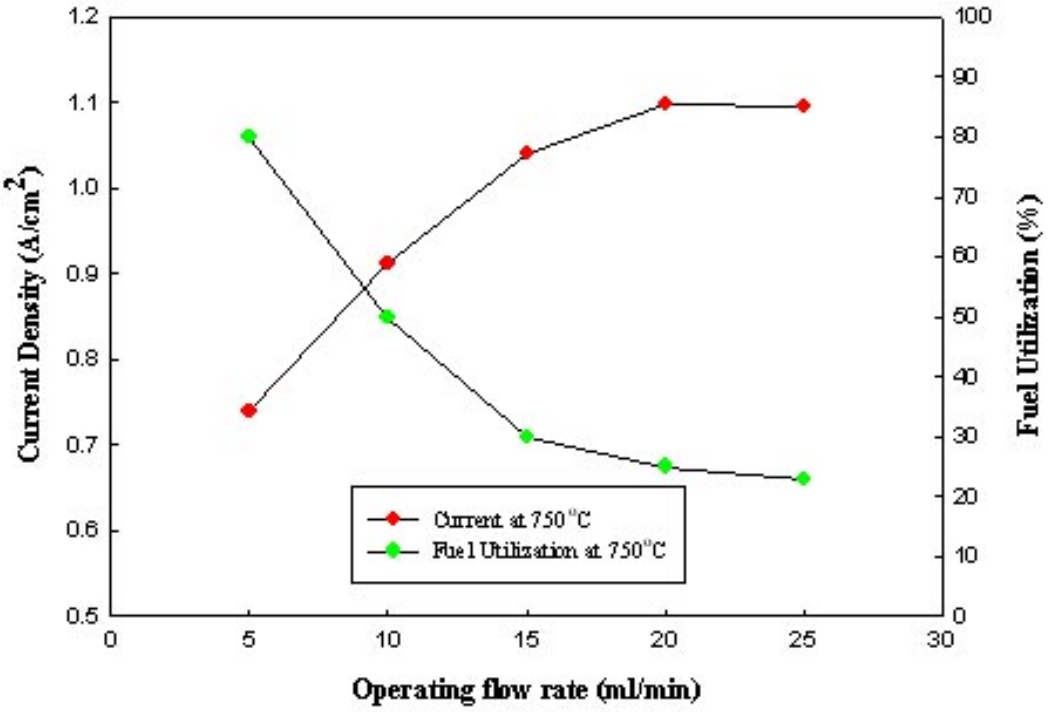

Figure 4.7 Influence of H_2 flow rate on current and fuel utilization at 750 ºC,0.5V

Figure 4.7 is the result for fuel utilisation at 750 ºC, 2hr reduction. The exhaust gas composition was measured using the mass spectrometer and the fuel utilisation was calculated from the equation:

Fuel utilisation = (fuel input – fuel in exhaust)/ fuel input

The result showed that fuel utilization fell rapidly as the hydrogen flow increased. 20 ml/min flow rate showed the best current output so it was decided to standardise the test procedure at 20ml/min, giving 25% fuel utilisation.

4.7 Influence of running temperature

Figure 4.8 showed that the current output was increased almost linearly with increasing running temperature. These result showed that as the temperature was raised from 750 to 850°C there was an increased current output of almost 27%, consistent with data from Kwon *et al* [152] which showed that the conductivity of YSZ doubles between 700 and 800ºC.

Performance was increased after each running cycle as temperature was raised and the highest current output was shown after 850ºC running temperature. However the nickel mesh and silver wires used in the fuel cell were affected by

increased temperature and over 900ºC showed severe damage as the melting point of silver was approached. These metal degradation effect can explain the drop in current above 900 ºC due to contact loss

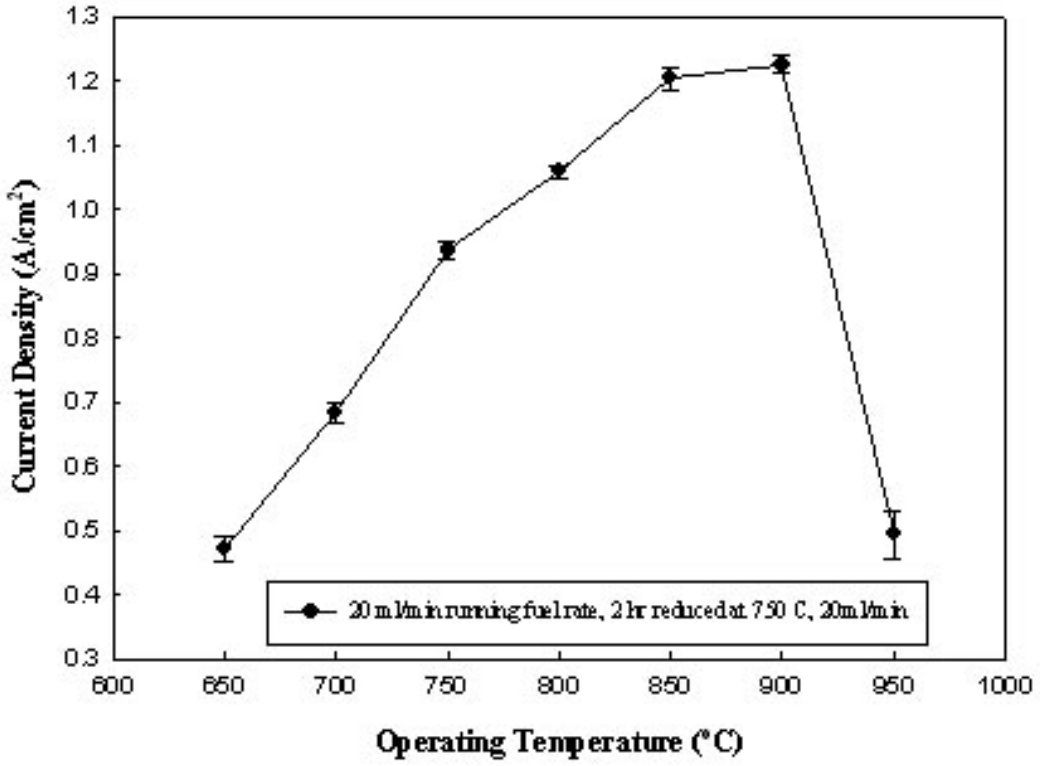

Figure 4.8 Current density for different running temperature at 0.5 V

4.8 Durability

One of the main problems in the cell was standardising the degradation of cell performance with operating time. Tests were carried out to show that the micro tubular cell did not degrade substantially over 500 minutes at 850°C (Figure 4.9).

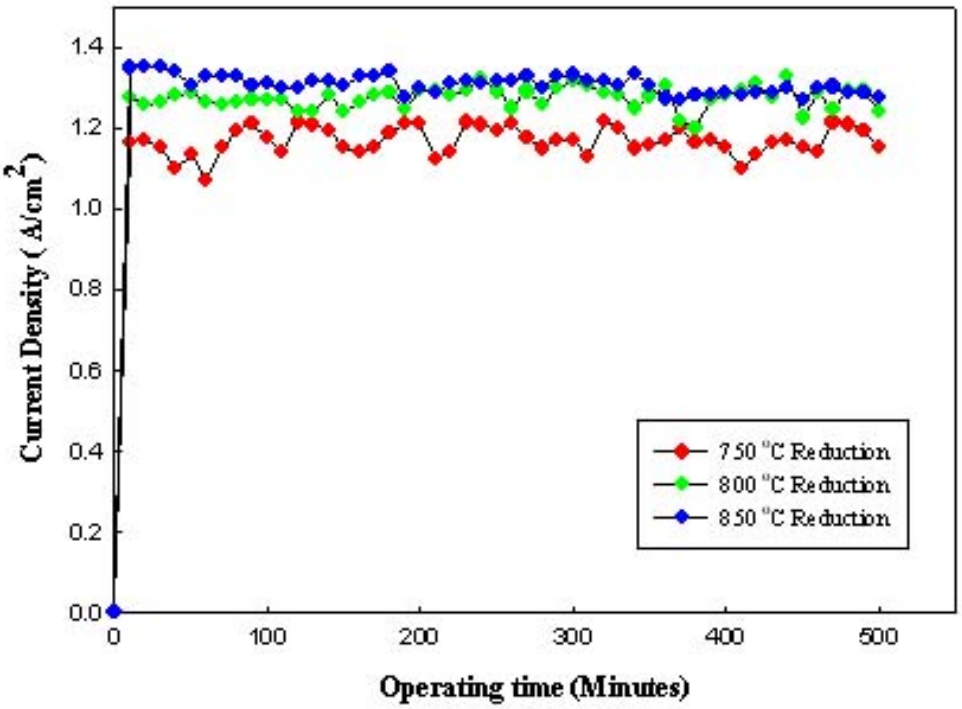

Figure 4.9 Performances of different reduction temperature with 20ml/min hydrogen at 0.5 V

The cell was tested with 20ml/min optimisation hydrogen flow rate condition as described above. The cells were set at 0.5V at 850°C and the current reading was recorded over time. It can be seen that almost stable performances were achieved in all conditions. High temperature reduced tubes showed an increase in current density by 13%. Over test periods of 500 min, approximately 4% degradation in performances was shown at 850°C reduction temperatures.

4.9 Conclusion

The reduction behaviour of SOFC tubular cells was studied under varying

temperature and hydrogen flow rate conditions to improve the performance of the cells. Both mechanical strength and current output of SOFCs were investigated and optimised.

From the result of the relation between reduction time and mechanical strength at 750°C and 20 min/ hydrogen, over 1 hr reduction time was necessary to give the best strength values.

The highest value of mechanical breaking stress was found between 102MPa and 138MPa after 1 hr reduction with 20ml/min of hydrogen and 750 °C temperature.

At 750°C, 2hr reduction led to the highest current output (approximately 1.14 A/cm^2) at 0.5 V. 20ml/min hydrogen flow rate was the optimal fuel flow rate for electrical performance.

The best performance followed a 2hr reduction at 850 ºC and 850 ºC running temperature with 20ml/min hydrogen flow rate.

Chapter 5

Anode Reduction on Pure Methane

5.1 Overview

This chapter reports the testing of a novel methane reduction method. Most previous investigations of SOFCs have been carried out using hydrogen as the fuel, and there is a relative lack of scientific literature on SOFC's using hydrocarbon as fuel, particularly involving any detailed catalytic, spectroscopic and structural characterization [153].

Moreover, there is no publication on methane reduction condition for subsequent operation on methane. Various methane reduction conditions can change the anode activity and this chapter investigates this effect. The theory proposed is based on the change in carbon deposition on the anode, depending on the reduction and operation parameters.

5.2 Experimental

The objective of these reduction experiments was to find the optimum conditions of temperature and flow rate using pure methane. Five cells were inserted into a silica tube placed in a furnace and various flows of methane were injected into the tube at several temperatures. 5 reduction conditions were studied at 10 ml/min methane flow an temperature of 650, 700, 750, 800 and 850^{o}C. Each condition was observed at four times; 15, 30, 45 and 60 min then mechanical strength

results were investigated. The cells were then measured for carbon deposition using TPO.

Electrochemical performance of the reduced cells was tested in a 20min period using the experimental setup shown in Figure 3.8. The fuel cell was heated to each target temperature in helium and then methane at 10ml/min was introduced. After open circuit voltage (OCV) was achieved, 0.5V was applied by potentiostat and the output current measured.

5.3 Three Point Bending Test

The strengths for different times of methane reduction at various temperatures are described in Figure 5.1. It was clear that 45min reduction was required to gain the best strength around 127 MPa. This was slightly lower than the strength achieved with hydrogen.

At the lower reduction temperature the strength was increased by 20% then there were no significant strength changes over 45 min. High temperature reduction between 45 to 60 min caused a mechanical strength decrease by 9%. This result indicated that the anode was being damaged by long time exposure to methane, giving gradual built up of carbon on the sintered anode. This

deposited carbon is known to push the anode grains apart to give anode damage and consequent lower strength [143].

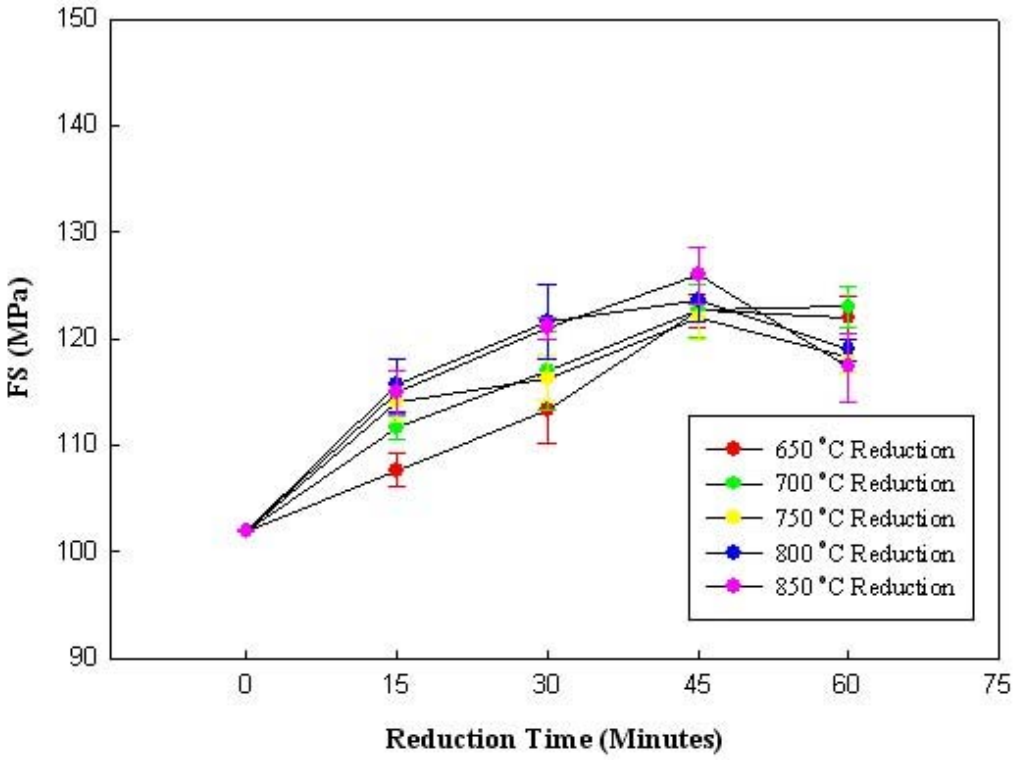

Figure 5.1 Mechanical strength of fuel cell with different reduction time and temperature at 10ml/min methane

5.4 Influence of Carbon Deposition in Different Reduction Time and Temperature on Methane

Figure 5.2 shows the effect of reduction conditions on carbon deposition measured by TPO. The mass of one cell Ni/YSZ cermet anode was 1 g. Each cell was cooled to room temperature and oxygen was passed through the cell. The

furnace was heated to 800 °C at a rate of 10 °C /min.

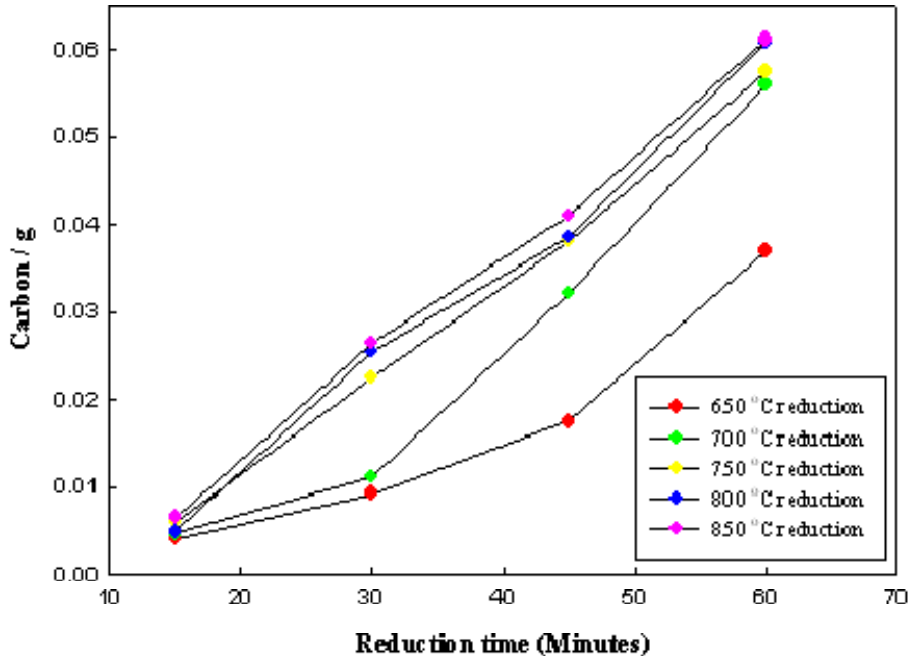

Figure 5.2 Carbon deposition results at five reduction temperatures with different reduction time.

The peak of CO_2 measured on the mass spectrometer trace was used to calculate the mass of carbon on the anode. It can be seen that carbon deposition had increased steadily with reduction time and temperature. Under the worst condition, 850°C for 60 min, 6% of carbon was coating the nickel and this caused anode damaged and blockage. The best reduction conditions were at 650°C and 700°C for 30 minutes, giving only 1% carbon on the anode.

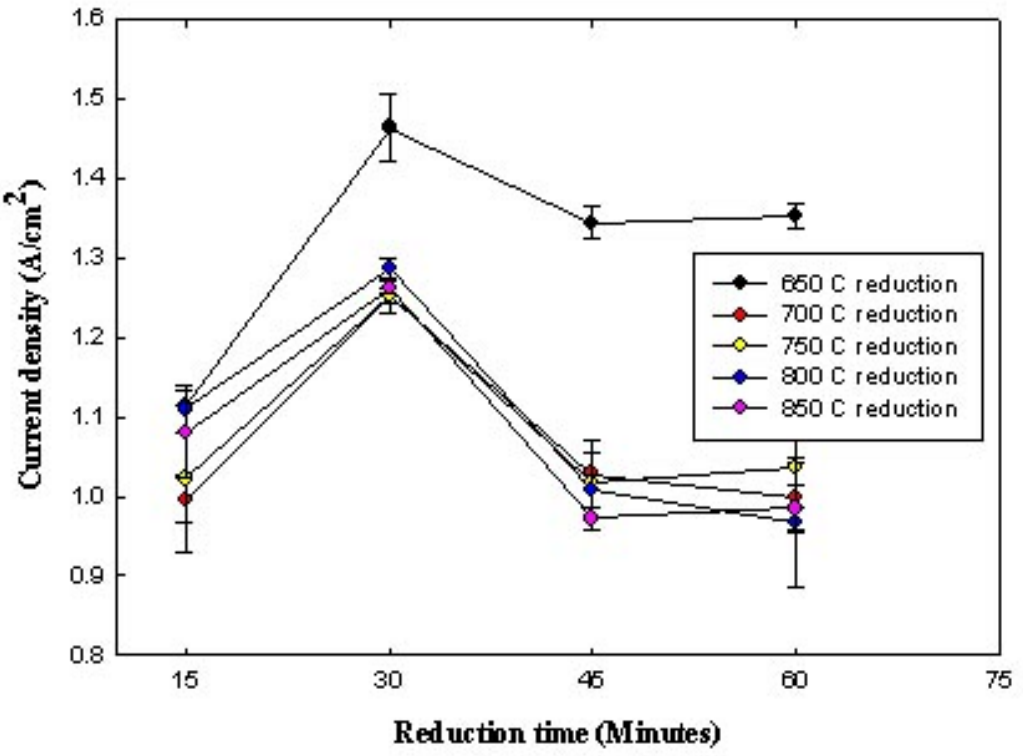

Figure 5.3 SOFC performances at 850 ^{o}C with 10 ml/min methane at 0.5 V after five different reduction times

This amount did not block the anode but instead enhanced the electrochemical performance as shown in Figure 5.3. These results suggest that coke builds up on the anode surface and this at first enhances electronic conduction but later pushes apart the nickel particle to give lower strength and poorer current.

Figure 5.3 illustrates the peak in electrochemical performance, measured at 0.5V and 850^{o}C in 10ml/min pure methane, for the anode reduced at 650^{o}C for 30 minutes. The current density was almost 1.45 A/cm^{2}, some 45% higher than the

high temperature reduction cells performance of 1 A/cm^2 at 0.5V. Compared with the hydrogen experiments in the last chapter, methane reduction condition showed 5% higher current output with reduction time lowered by up to 300%.

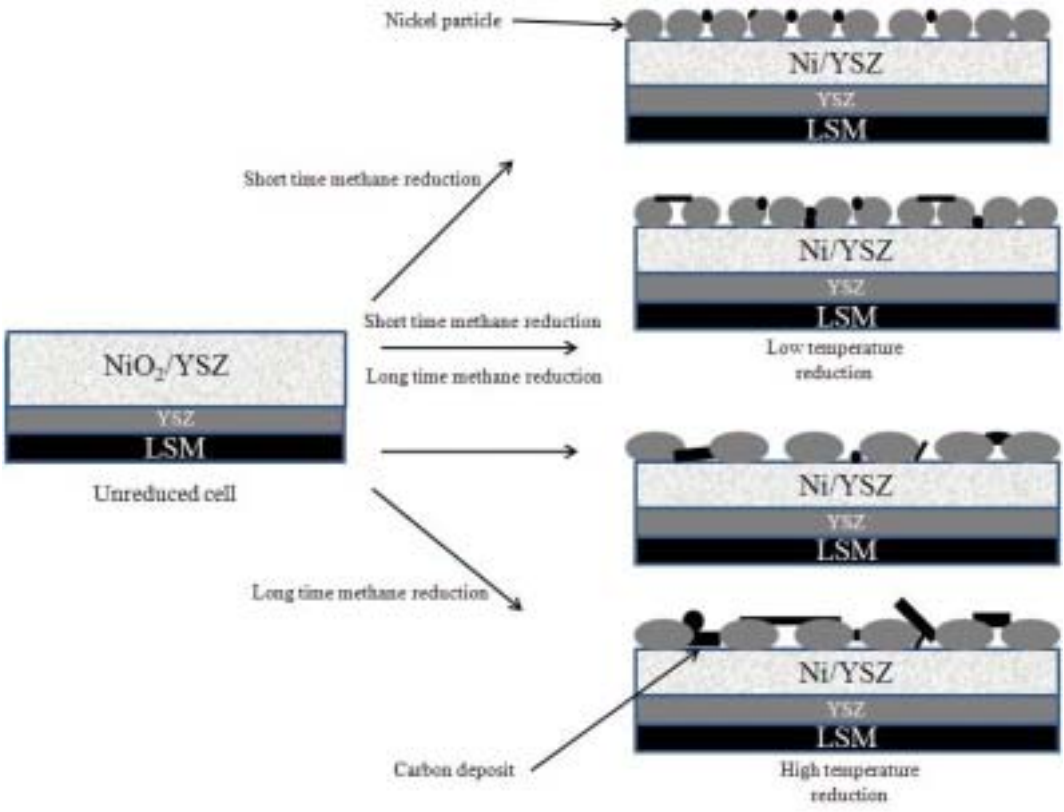

Figure 5.4 Proposed anode structures after different time and temperature

This is a significant result because it shows that the deposition of carbon under optimum conditions can have a beneficial effect. This can be explained by the increased catalytic activity of the anode due to the finer particles after low temperature reduction. Also the current output was affected by reduction time.

From 30min to 60min reduction, the performance was degraded up to 26%. Figure 5.4 illustrates the model of carbon affecting the anode structure under the different conditions.

In the short time methane reduction at low temperature, smaller nickel particles are formed and these tend to be separated, which causes electronic conductivity to be low. Introducing short time methane reduction causes small amount of carbon to be deposited which improves the conductivity. Under these circumstances, the Ni/YSZ cermet anode is viewed as a composite of Ni particles connected by C nanostructures which provide improved electrical connection and robust mechanical and thermal properties [139,154-155].

The large nickel particles activity and does not get blocked by carbon deposits. However at long time methane reduction, carbon deposition is generated partially on the anode surface, blocking it and hence leading to degraded current output.

At high temperature reduction, both long and short time reduction showed the carbon deposition and carbon was depositing denser than at low temperature. From the above results, 30 min reduction time at 650^{o}C with 10ml/min methane

was the optimum condition for electrical performance of SOFCs. Further anode surface analysis will be mentioned with SEM and EDX in chapter 5.6

5.5 Influence of Reduction Flow Rate

The behaviour of cells prepared by different reduction methods was investigated using methane. Figure 5.5 shows the effect of different methane flow rates during the reduction process. The cell was reduced at 4 different methane flow rates; 5, 10, 15 and 20 ml/min at the optimum reduction condition of 650^{o}C for 30 minutes.

5 ml/min reduction flow rate gave a low output, while 10 ml/min gave the best output. All cells performed reasonably well during short term periods. However, the cell showed signs of degradation when the cell was reduced under high flow rate. Raising the reduction methane flow rate from 10 to 20ml/min degraded the power output (up to 7%), suggesting that carbon was depositing too thickly and blocking the Ni catalyst sites. However, these results do not show any evidence of cell micro-cracking. Cell failure by cracking was often observed after 40 min cell operation because of the carbon deposition.

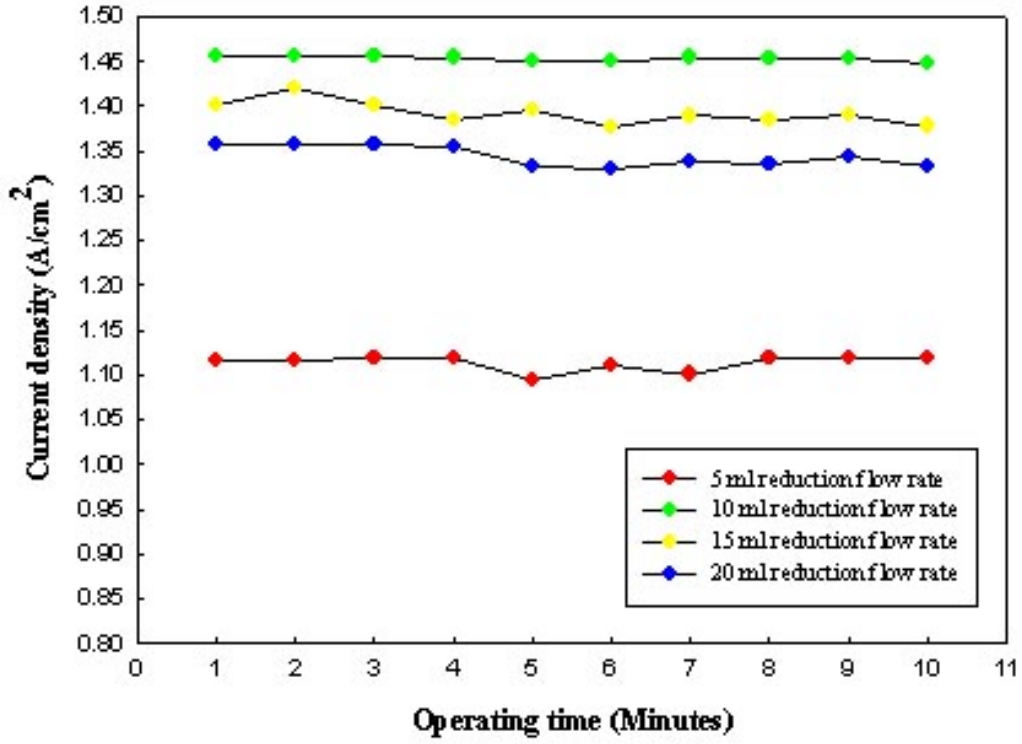

Figure 5.5 Current output after optimum reduction with different reduction flow rates on methane

5.6 Characteristic of Anode Surface

The anode surface after two different reduction methods samples was investigated by SEM and EDX

Low temperature reduction samples: 10ml/min, 650^{o}C reduction temperature in 30 min and 60min reduction time

High temperature reduction samples: 10ml/min, 850^{o}C reduction temperature in 30 min and 60min reduction time.

5.6.1 Low Temperature Reduction

Figure 5.6 and 5.7 taken from a region near the anode surface, shows clear evidence of carbon: The EDX spectrum showed an increased carbon wt% while reduction time was increased between 30 min and 1 hour reduction time. The cell was reduced at 650 ^{o}C using 10ml/min flow rate.

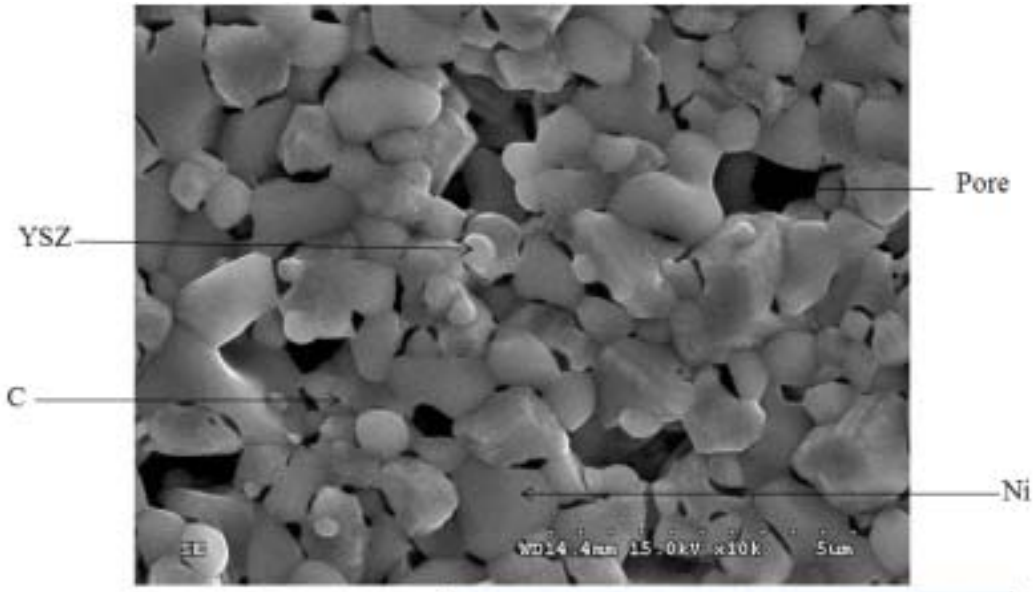

Element	Weight %	Atomic %
C	0.93	3.59
O	13.58	39.41
Ni	47.67	37.70
Y	4.09	2.13
Zr	33.73	17.17
Total	100.00	

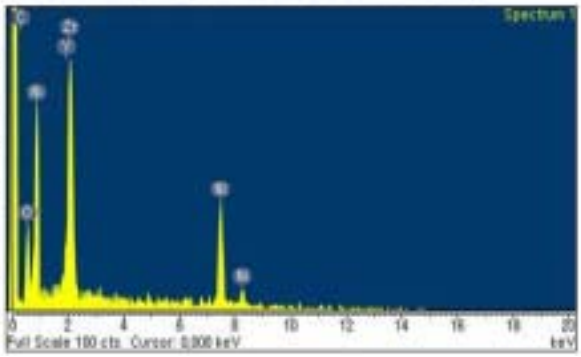

Figure 5.6 650^{o}C and 10ml/min methane reduction results of SEM and EDX at 30 min reduction

Figure 5.6 showed that a small amount of carbon particles (0.93 wt%) was deposited on the anode structure and this linked the anode Ni particles,

improving electrical conductivity and thus increasing current output in Figure 5.3 When the cell was reduced over a long period (1 hour reduction) carbon deposition was increased by 3 wt% on anode surface (Figure 5.7). At 30 min reduction, the anode surface showed a smoother profile, indicating finer particles.

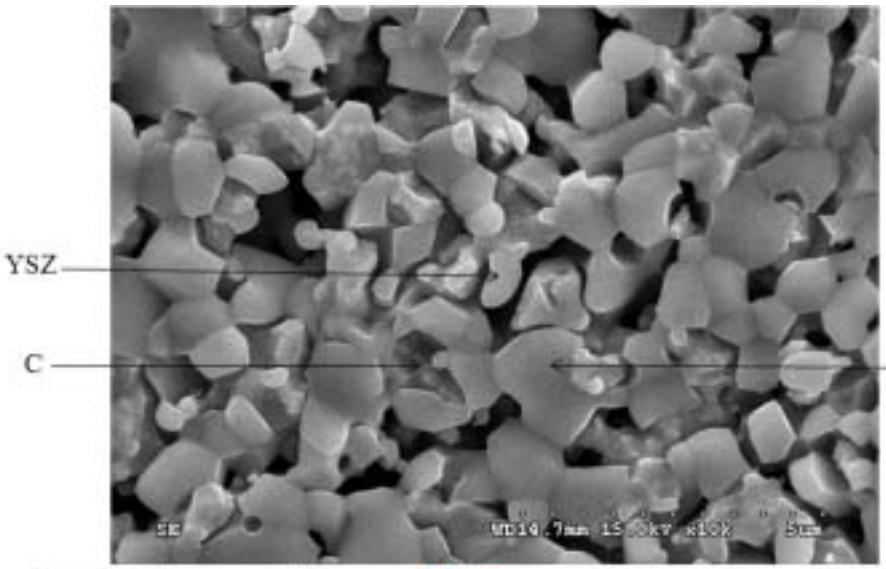

Element	Weight %	Atomic %
C	4.34	16.45
O	9.50	27.02
Ni	48.72	37.76
Y	7.30	3.73
Zr	30.14	15.04
Total	100.00	

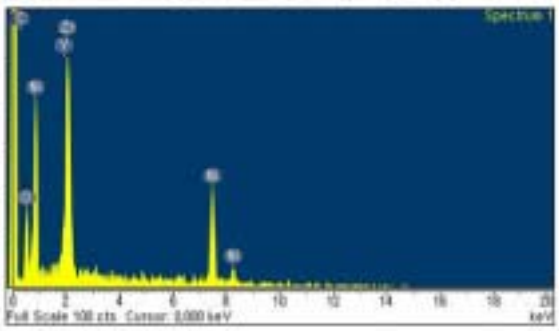

Figure 5.7 650^{o}C and 10ml/min methane reduction results of SEM and EDX at 1hr reduction

SEM-EDX results showed very small C peaks both at 30 min and 60 min. At 30 min reduction, Ni particles are well dispersed and small carbon deposition gave improved connection.

This small amount of carbon deposition found in the anode working surface was consistent with the improved current outputs. As mentioned earlier, small levels of carbon deposition have been shown to be beneficial to cell performance.

Depending on the method of manufacture the Ni particle size may vary from nanometers to micrometers. Figure 5.6 showed small Ni particles following optimum reduction time condition. In contrast Figure 5.7 showed increased carbon deposition after 1hr reduction, leading to poor current output.

5.6.2 High Temperature Reduction

EDX measurements were taken after 850^{o}C, 10ml/min methane reduction with 30min and 1hr time conditions. Figure 5.8 showed that two effects had occurred: first the carbon level was high leading to damage: second the nickel had aggregated into larger clump.

Despite a small C peak shown at 30min methane reduction the coking occurred on several parts of the anode layer. However a strong C peak was showed in Figure 5.9 (1hr reduction condition). These results suggest that coke builds up within the anode. At high temperature, carbon may block anode pores, degrading cell performance. Also the coke buildup may lead to volume expansion and

consequent micro-cracking. However there is no evidence of micro cracking in the SEM image.

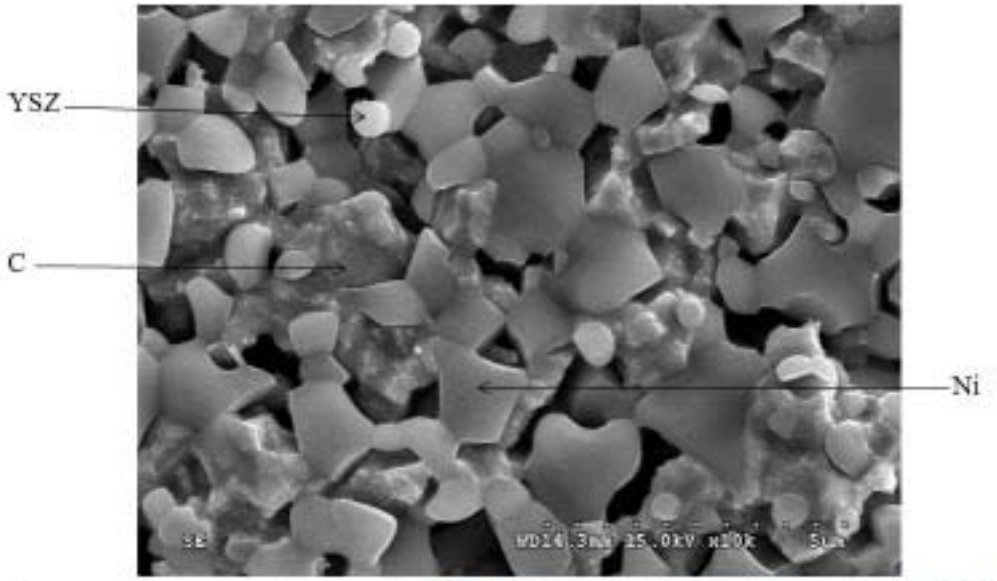

Element	Weight %	Atomic %
C	4.91	16.34
O	12.67	33.58
Ni	41.59	31.04
Y	4.38	2.09
Zr	36.46	16.95
Total	100.00	

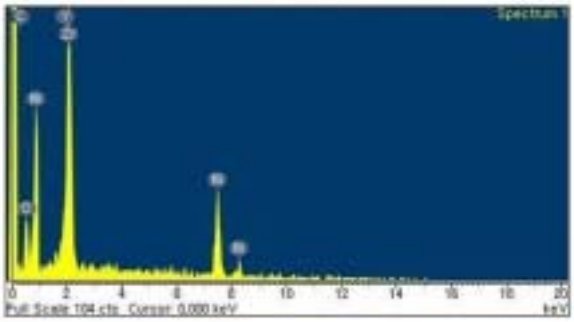

Figure 5.8 850°C and 10ml/min methane reduction results of SEM and EDX at 30 min reduction

This may lead to an interruption of anode current collection pathways. This behaviour supports strength results (Figure 5.1) and low current output (Figure 5.3). From 30 to 60min, increased 35 wt% C element was shown on the anode surface. Compared with 30min reduction temperature deposition, the wt% was significantly increased by 38%.

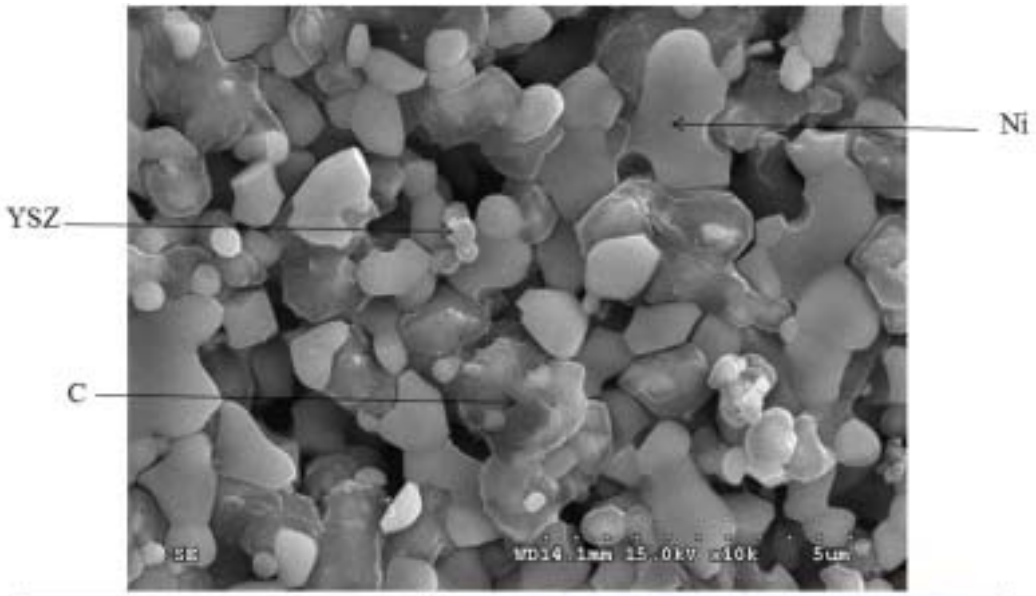

Element	Weight %	Atomic %
C	38.98	72.30
O	8.00	11.14
Ni	26.46	10.04
Y	4.39	1.10
Zr	22.18	5.42
Total	100.00	

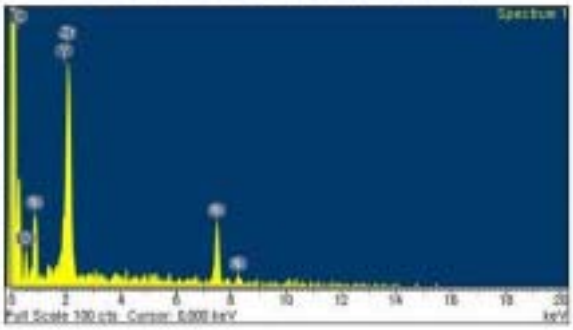

Figure 5.9 850°C and 10ml/min methane reduction results of SEM and EDX at 1hr reduction

Figure 5.9 shows that the carbon particles may block anode pores and it may lead to volume expansion. This significant carbon deposition produced interruption of anode current pathway. No oxygen is supplied by a electrochemical reaction and therefore carbon is formed due to the cracking of methane. This behaviour can lead to the cell failure and micro-cracking, cell failure by cracking will be shown in short term periods. This can be explained by the decreased nickel % of the anode. Further investigation will be described in

chapter 6.

5.7 Conclusions

This chapter has demonstrated the effect of methane on both the reduction and operation of nickel/YSZ anodes in microtubular SOFCs. At all temperatures, the mechanical strength results showed that reduction condition for 45 min with 10 ml/min methane was the best condition. Compared with hydrogen, strength was decreased by up to 25%, suggesting some damage due to carbon deposition.

Low temperature (650°C) with short time (30min) reduction time, 10ml/min methane flow rate led to the lowest carbon deposition (1 % carbon) and Ni particles were found to be dispersed on the anode surface and separated for maximum surface area. But the carbon had connected the Ni grains to give reasonable electronic conduction.

The best performance with methane reduction condition of 1.4 A/cm^2 at 0.5 V was achieved at 650°C with 10 ml/min flow rate. SEM and EDX results showed that there was evidence of 1% carbon deposition at low temperature with short time reduction.

Chapter 6

Methane Operating Parameters after Methane Reduction

6.1 Overview

In this chapter, the objective was to derive the optimum operating conditions for the microtubular SOFC running on methane after reduction on methane to contrast with hydrogen base results. Optimum methane reduced cells were operated at various temperatures and several methane flow rates. The aim of this chapter was to find an optimum combination of operating conditions for best performance without excessive carbon deposition on the anode whilst maintaining acceptable fuel utilization and exhaust composition.

6.2 Experimental

The optimised reduction condition of 650^{o}C for 30 minutes at 10ml/min methane was used in most of these tests. The optimum was studied at various flow rates and operating temperature. Also the worst reduction condition, 850^{o}C at 20ml/min of methane, was investigated.

Each condition was observed during four runs then the carbon deposition on the anode was investigated using TPO, SEM and EDX. Electrochemical performance of the cells was tested using the experimental setup shown in Figure 3.8. The fuel cell was heated to 850^{o}C and then methane was introduced. After OCV was achieved, a load of 0.5V was applied.

6.3 Influence of Operating Temperature

As shown in Figure 6.1 the operating temperature affected the performance of the cell in the expected manner, the output current rising rapidly with temperature above 450 ^{o}C above and levelling off about 850 ^{o}C.

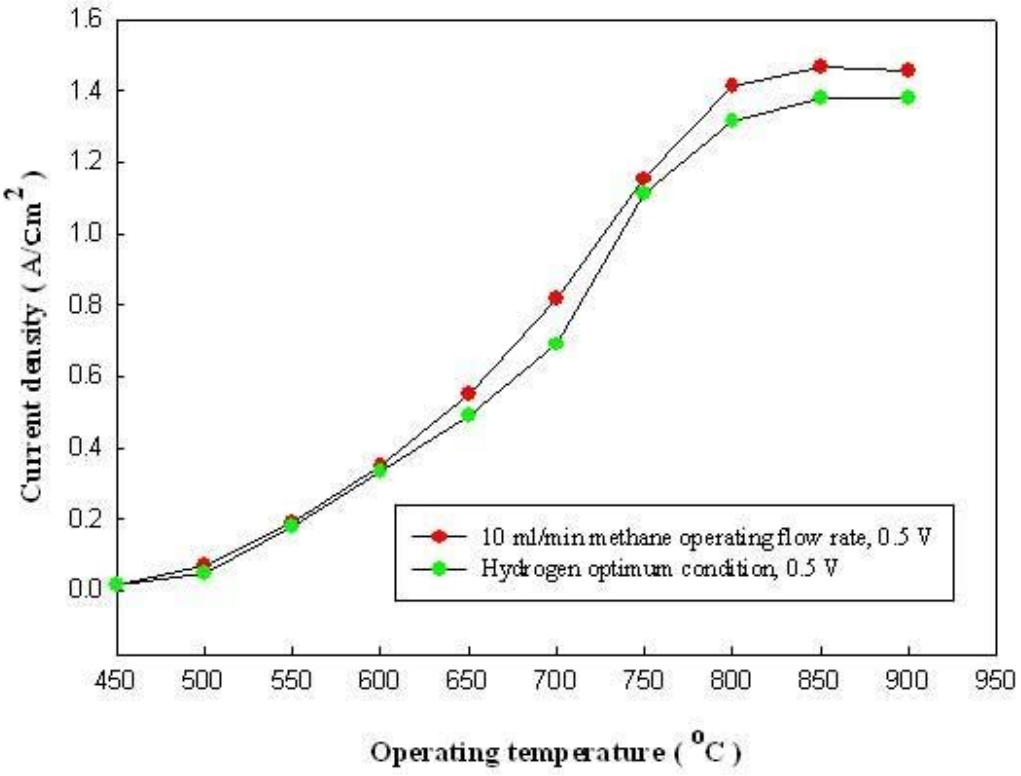

Figure 6.1 Current density for different running temperature at 0.5 V

The poor current output at low temperature was predominantly a direct consequence of the inability of the cathode and electrolyte to capture and conduct oxygen ions below 600^{o}C. Over 850 ^{o}C there was no significant change of current

because the conductivity of both cathode and electrolyte became constant [151]. By comparing with the optimized current output using hydrogen as fuel it may be seen that pure methane can give slightly better power output over the whole temperature range.

6.4 Influence of Running Flow Rate

The difference between methane and hydrogen operation became clear when increased flow rates of methane were tested as shown in Figure 6.2. 2.5ml/min methane flow gave a current of 1.17 A/cm^2 when running for 10 minutes.

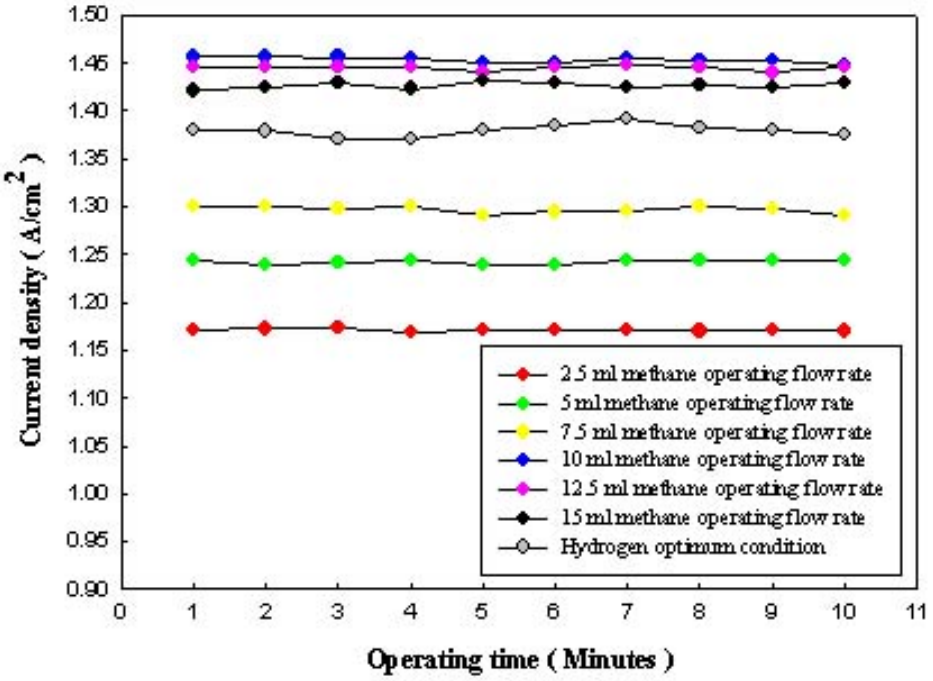

Figure 6.2 Current density measurement after optimum reduction with different operating flow rates on methane

Raising the methane flow rate, ie decreasing the fuel utilisation, gave increased current as expected, but it was found that 10ml/min gave the maximum current, after which further increasing of methane flow gave a decreasing power, indicating that carbon deposition was beginning to block the catalyst. Comparing with hydrogen optimum condition, 10ml/min methane operating condition gave better power output by up to 5%.

When dry methane gas is used as a fuel, carbon particles are created on the anode surface, but steam is also generated by the reaction of methane with oxygen emerging from the YSZ at the anode. This steam reaction product will reform the methane at a rate which depends on the gas flow [18, 19].

Those reports showed that methane was completely oxidized to carbon dioxide and water without carbon deposition on the anode surface at low methane flow rates. Figure 6.2 showed similar result that the 2.5ml/min condition where the output remained steady.

Fuel utilization was investigated with methane using the same method as described in chapter 4.6. Figure 6.3 shows that 10ml/min flow rate gave 41% fuel utilization after optimum reduction.

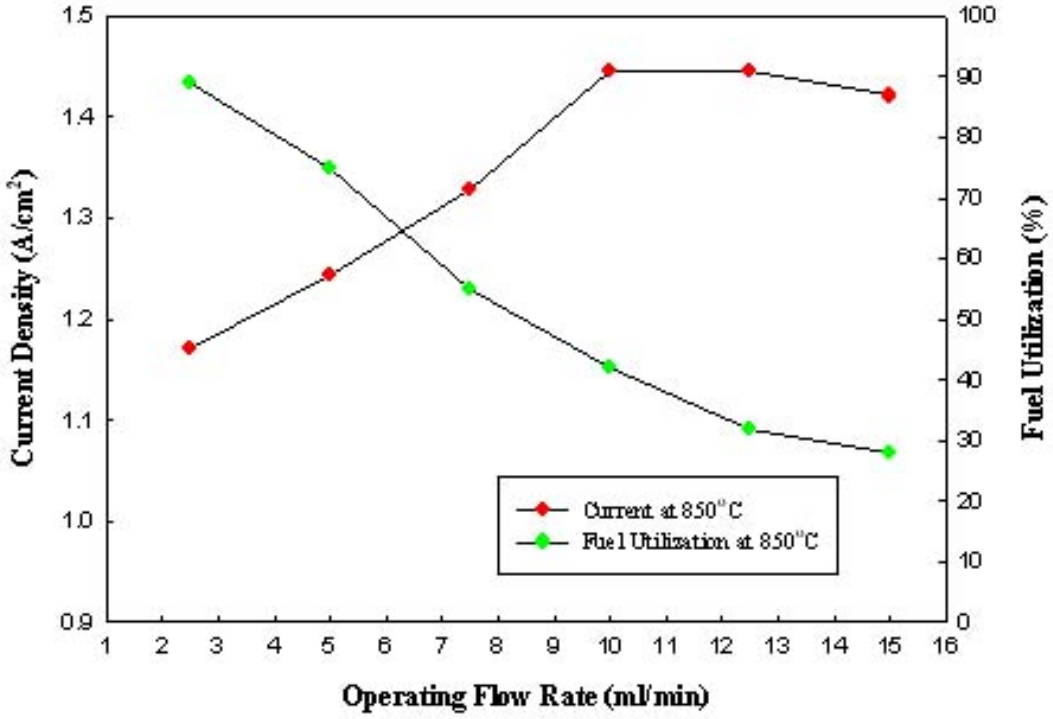

Figure 6.3 Influence of CH_4 flow rate on current and fuel utilization at 850 °C at 0.5V

6.5 Durability

The main problem of methane operation is durability because of carbon deposition causing anode damage [3-4]. Therefore three separate durability experiments at 850 ^{o}C were carried out with different methane flow rates from 5 to 15ml/min (Figure 6.4). Cells were reduced at the optimum methane conditions ie 30min, 10ml/min , 650^{o}C.

In the first 40 minutes approximately 12% initial degradation was observed for all the cells, indicating anode sintering. After 40 minutes, the current stabilised

and gave almost steady current output over 500 minutes period for the 5 and 15 ml/min experiments. The carbon deposition did not hinder the performance.

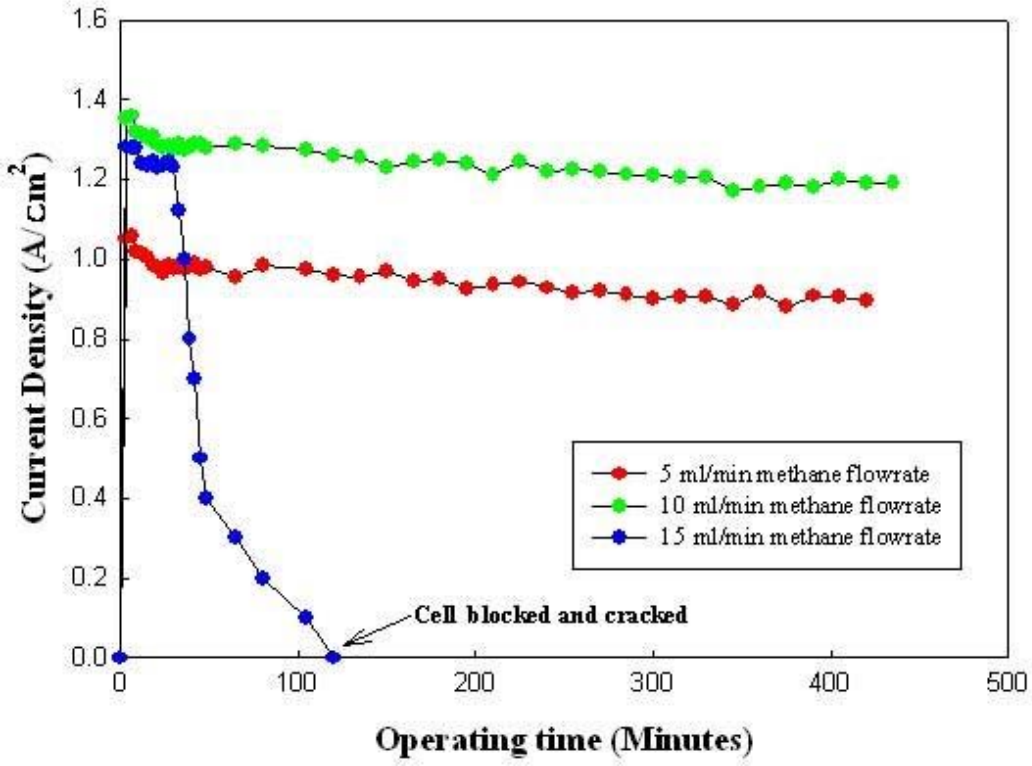

Figure 6.4 Performance of different flow rate at 850 ºC with optimum reduction, 0.5 V

However, 15ml/min flow rate gave a rapid drop in current after 100 minutes with zero output after 2hrs. Eventually, the anode became completely blocked by carbon under this operating condition. The high operating methane flow rate must have cause continual carbon deposition on the nickel anode, eventually leading to a thick coating together with anode disruption and cell failure. The

anode was obviously damaged because the high current output could not be recovered from the cell after the carbon was oxidised away by heating in air.

6.6 Characteristics of Anode Surface by electron microscopy

After the 500 minutes durability test, the anode surface was investigated by SEM and EDX.

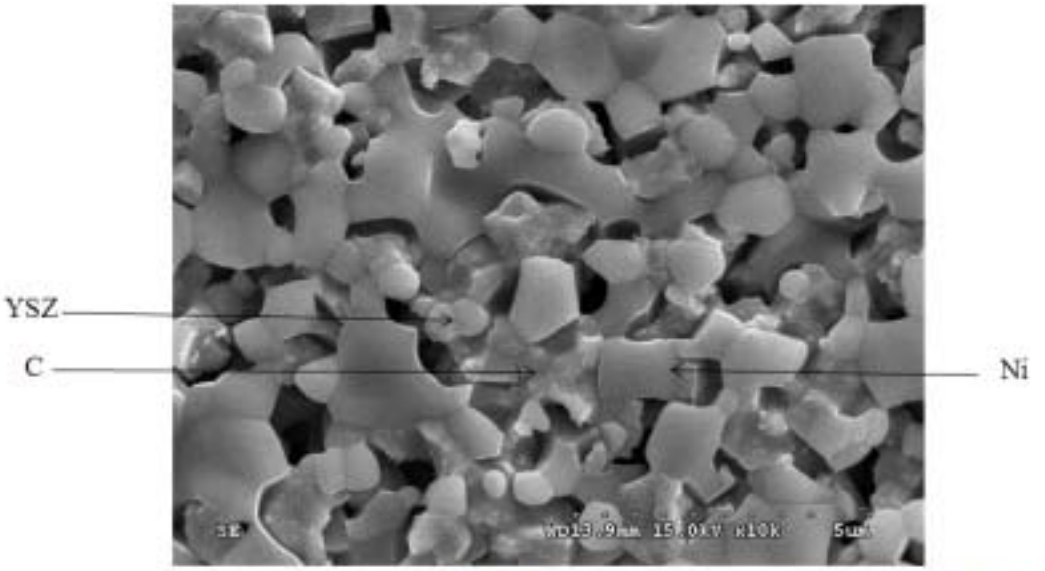

Element	Weight %	Atomic %
C	3.54	12.57
O	14.30	38.11
Ni	42.00	30.49
Y	5.60	2.69
Zr	34.56	16.15
Total	100.00	

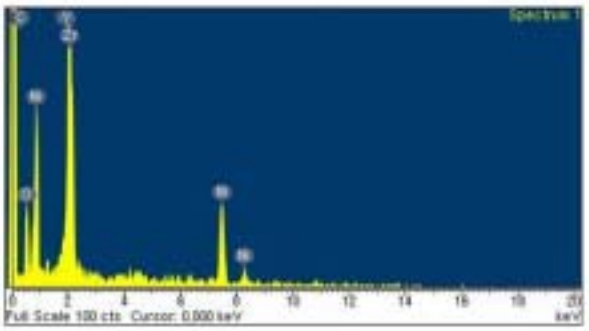

Figure 6.5 Anode surface after 500 minutes test with 10ml/min methane operating flow rate under optimum reduction.

Figure 6.5 shows the anode surface covered with small amounts of carbon particles. Because the carbon particles were well deposited in anode pores the coke was hard to find in this SEM image. These tended to be separated from the nickel particles and there was no evidence of carbon agglomeration to cause cell blockage. Although the carbon signal was 3.5% this was clearly insufficient to destroy the cell performance.

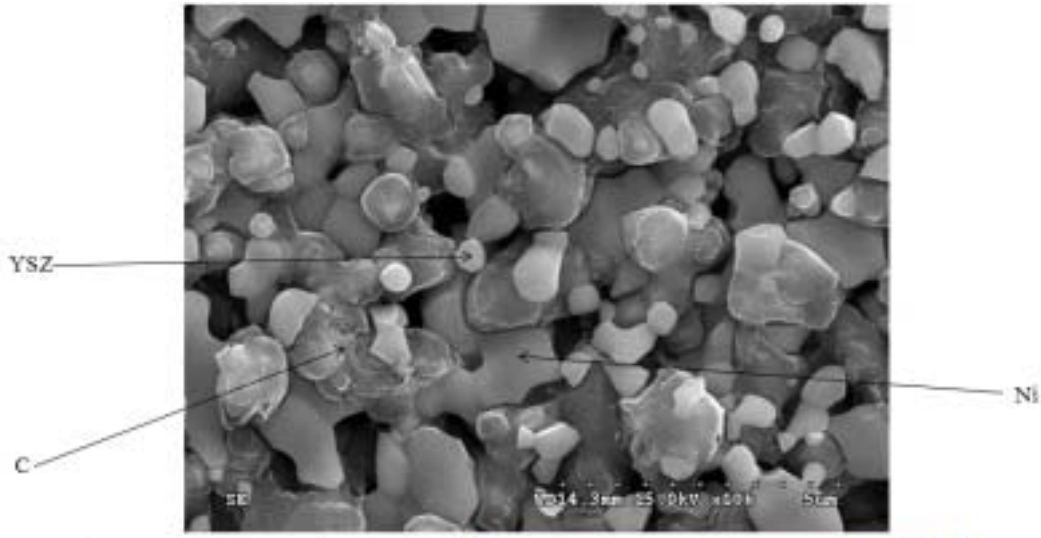

Element	Weight %	Atomic %
C	48.49	81.52
O	3.90	4.92
Ni	24.47	8.42
Y	1.91	0.43
Zr	21.23	4.70
Total	100.00	

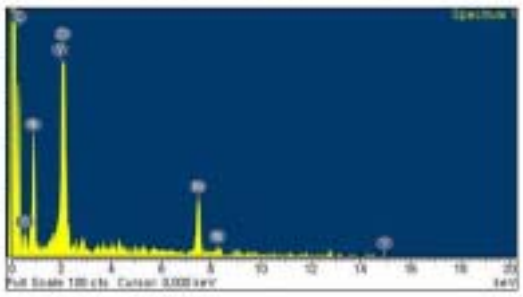

Figure 6.6 The anode surface after 100 minutes test at the zero current output.

Figure 6.6 SEM image was taken after 15ml/min operation for 100 minutes. It showed a very high carbon signal indicating that the anode had been blocked to

give zero current. The surface structure was now seen to be dominated by carbon depositions, thus explaining the zero current output.

These results showed that the microtubular SOFCs could be operated on pure methane but flow rate was crucial and had to be maintained below 10ml/min. Additionally, it was vital to draw current from the cell to oxidise any carbon depositing on the anode

6.7 Carbon Deposition on anode measured by mass spectrometer.

The carbon deposition was measured by mass spectrometry using temperature programmed reaction after 500 minutes tests with different methane flow rates.

The peak of CO_2 measured on the mass spectrometer trace was used to calculate the mass of carbon on the anode (Figure 6.7). It can be seen that carbon deposition had increased significantly at 15 ml/min to give the blocked cell during 40 minutes operation. 7% of carbon was coating the nickel, much more than that on the cells running at 5 and 10 ml/min.

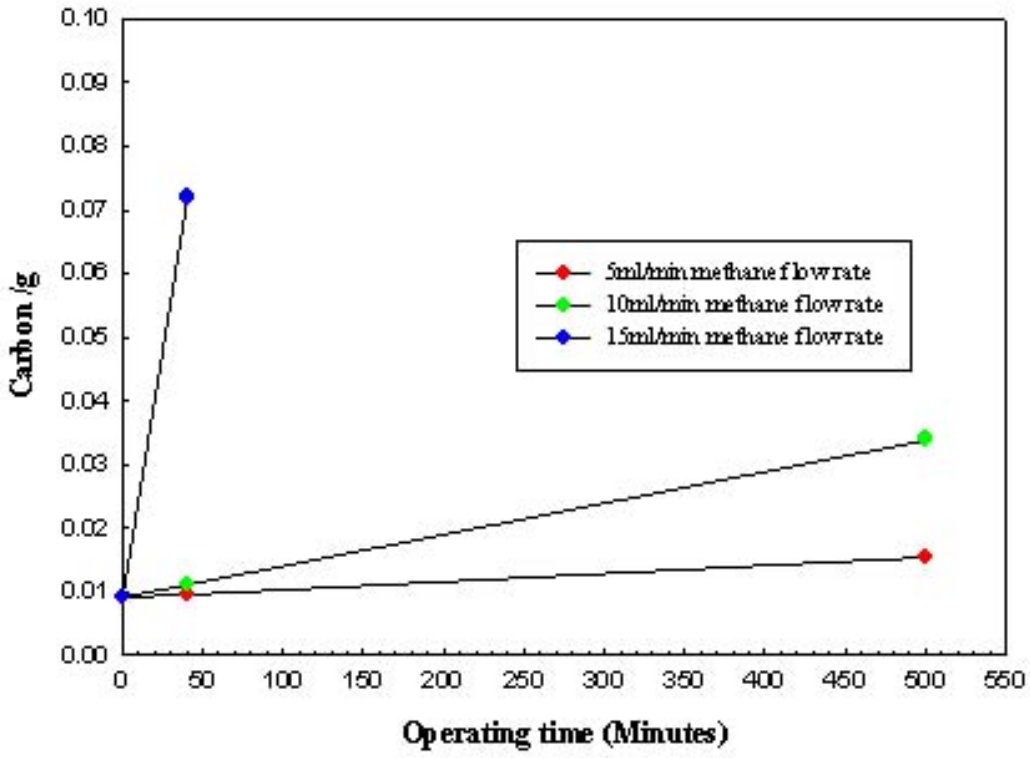

Figure 6.7 Carbon depositions at 850 operating temperature with different flow rates under optimum reduction condition after 500 min operation at 0.5 V

As mentioned earlier in chapter 5, 6% carbon deposition caused blockage on the anode. The best operating conditions were at 10 ml/min methane flow rate giving 1.1 % carbon deposition on the anode in 40 minutes. After 500 minutes running on 10ml/min methane, the carbon deposition was increased to 3.4 %. But this did not block the anode and gave steady electrical performance as shown in Figure 6.4. 10ml/min operating flow rate therefore showed the best current output. It is important to demonstrate that the amount of carbon on the anode can be maintained constant over long periods of use. It was shown that

when the cell operated under 5ml/min methane operating conditions the tubes ran successfully even with carbon deposition because the small amount of carbon deposited was linking the nickel particles to give improved conductivity, but without damaging or blocking the structure.

6.8 Hydrogen and Methane Optimum Condition

Figure 6.8 shows the cell output current density for both hydrogen and methane optimum conditions.

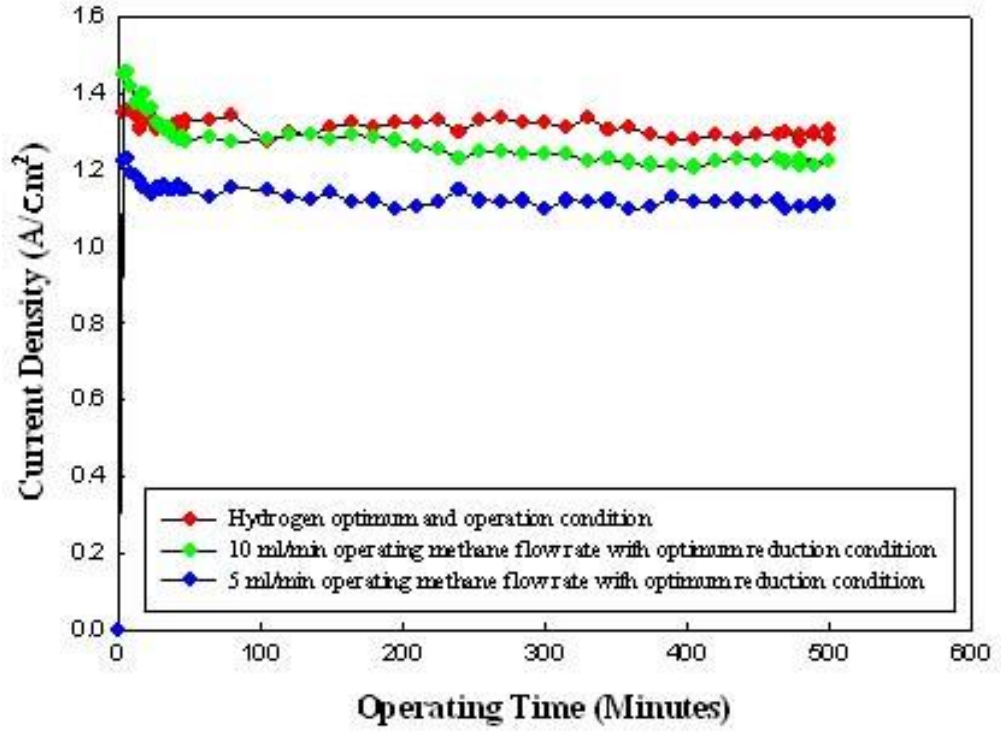

Figure 6.8 500 minutes testing of hydrogen and methane optimum condition

The cells running on hydrogen produced steady current then declined by 6% as

the anode sintered. The optimum methane condition was shown to be 7% better than hydrogen condition in the first 100 minutes as a result of the early deposit of carbon on the anode from methane reduction.

It was clear that the current output on methane was diminishing as the test proceeded suggesting that further damaging carbon build-up was take place. Therefore, the flow-rate was reduced to keep the output constant. This was found to occur at 5 ml/min. In a previous published paper [142], this low operating flow rate showed steady current output without carbon deposition over long periods.

This result shows that the fuel cell can operate for long periods without carbon damage, providing the methane flow-rate is controlled at a suitable level and that there is sufficient current flow through the fuel cell to oxidise any carbon building up on the nickel with time.

6.9 Conclusions

Results of this chapter have shown the best performance operating condition on pure methane.

The optimum running condition at 850^{o}C was found to be 10ml/min methane flow rate. Methane has been shown to outperform hydrogen by up to 7% in the first 100 minutes but it had a possibility of blocked anode surface over long periods test. However 5ml/min flow rate of gas showed that methane was giving low carbon deposition on the anode surface at low flow rate and steady electrical performance without excess carbon deposition, over long periods..

Chapter 7

Conclusions and Future Work

7.1 Summary of Conclusions

The optimisation of both hydrogen and methane reduction and operating experiments have been conducted in order to improve the performance of anode supported micro tubular SOFC. The conclusions of this thesis are:

1. Hydrogen reduction and operation: mechanical strength and current output of SOFCs were investigated. Reduction at low temperature gave poor output performance and mechanical strength, but the performance was very good when the tubes were reduced at high temperature over 800°C. The optimum condition was over 1hr reduction condition at high temperature.

   The highest value of strength was found between 102MPa and 138MPa after 1 hr reduction with 20ml/min of hydrogen and 750°C temperature. The subsequent cell performance was a 1 A/cm^2 at 750°C and rose to 1.25 A/cm^2 at 850°C.

   The highest current density was obtained at 850°C and 20 ml/min flow rate. However, the cell gave poor performances over 900°C due to the melting temperature of silver current collector.

2. Methane reduction: The cell was tested under varying reduction conditions and the effects of reduction on the anode surface were investigated. The best reductions conditions were at 650^{o}C for 30 minutes with 10ml/min flow, giving only 1% carbon on the anode, which enhanced the electrical output. The carbon appeared to protect the nickel particles from sintering, while aiding the electronic conduction between the Ni particles. Longer reduction times caused increased carbon depositions which tended to block and damage the anode.

3. The deposition of carbon under optimum conditions can have a beneficial effect which can be explained by the increased catalytic activity of the anode after low temperature reduction. At high temperature reduction, coke build up, shown by a strong peak carbon in EDX, within the anode and anode was damaged. Carbon deposition was affected by reduction temperature.

4. Methane operation as a fuel: The optimum operation condition was investigated after reducing at 650 ^{o}C for 30 minutes in 10/min methane, the best reduction condition. Compared to hydrogen operation, the current was increased significantly at 0.5 V over the whole temperature range.

Over 800^{o}C, 10ml/min flow rate, the performance peaked at 1.43 A/cm^{2} at 0.5V in short term operation.

At low operating flow rate, it was shown that methane was completely oxidized to carbon dioxide and water without carbon deposition on the anode surface. At high flow rate, methane flow gave a diminishing performance with time owing to carbon damage to the Ni anode.

5. The 500 minutes operating test showed that cell performance was strongly affected by methane flow rate during operation after optimum reduction condition. At 15ml/min and 850^{o}C, cell was blocked in the first 40 minutes and carbon deposition was increased by 620%. At lower flow rates, the cell was successfully operated for much longer testing periods because carbon did not build up. The SEM image and EDX data supported these results.

6. In all experiments, there was a pre-deposit carbon effect from methane reduction, and cells then showed 7% higher current output compared to hydrogen conditions. Comparing with hydrogen operation, methane performed better than hydrogen in the first initial performance but declined if carbon was allowed to deposit with time

It is clear from these results that pure methane can be used both as a reductant and a fuel for operating anode supported microtubular SOFCs in contrast to previous reports where the cell was reduced on hydrogen and subsequently operated on methane. Reduction and operation on methane can give performance benefits while eliminating the need for additional infrastructure for hydrogen supply in buildings.

7.2. Future work

1. To investigate the effect of methane condition for other anode materials. Several materials such as Pt and Ru need to be tested to compare with the standard Ni-YSZ anode.

2. This thesis has shown the possibility of methane reduction and operation. Further work needs to be conducted to investigate the effect that carbon has on the anode during redox temperature cycling.

3. Figure 7.1 shows the preliminary result of the hydrogen operation of the microtubular SOFCs after optimum reduction with methane. This result showed higher current output than expected. Further investigation is needed into this through SEM and fuel cycling.

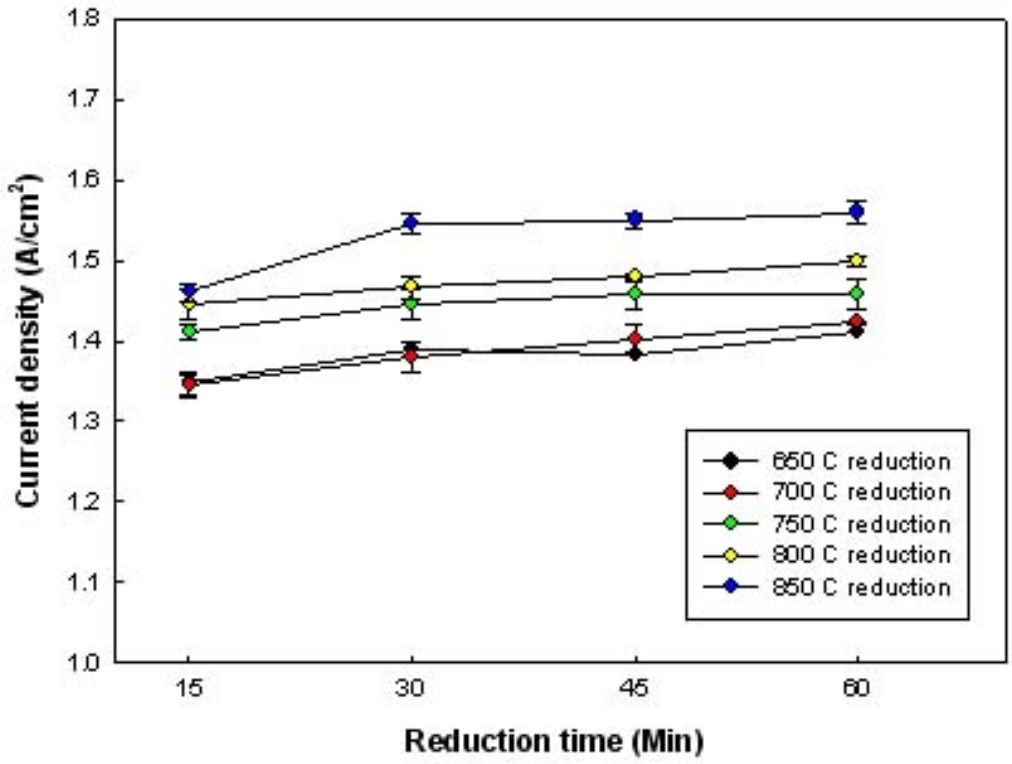

Figure 7.1 SOFC performances at 850 ^{o}C with 20 ml/min hydrogen at 0.5 V after five different methane reduction.

4. Further improvement is still needed in the design of the cells. It was shown that the cathode and electrolyte hinder the performance at lower temperatures. Hence alternative cathode compositions should be considered.

5. To develop a better anode interconnect (pin and cage) which remains securely inside the micro-tubular fuel cell and thus allows redox temperature cycling (for example Ag paste).

6. During 500 min test (Figure 6.6), the carbon deposition was significantly increased by the increased flow rate. To investigate the rate of carbon deposition, the cell is needed in long term period (over 1000 hr) test with low flow rates.

7. Other higher hydrocarbons fuel reduction and operation conditions need to be tested to compare with methane. This is important because natural gas which is available in many homes contains significant amounts of ethane, propane and higher hydrocarbon.

References

1. S. Singhal, and K. Kendall, *High Temperature Solid Oxide Fuel Cells: Fundamentals, Design and Applications*. 2003: Elsevier Advanced Technology, Oxford.

2. J. Liu, S.A. Barnett, Solid State Ionics, *Operation of anode-supported solid oxide fuel cells on methane and natural gas.* 2003, 158(1-2), p. 11-16.

3. C. M. Finnerty, N.J. Coe, R.H. Cunningham, R. M. Ormerod, *Carbon formation on and deactivation of nickel-based/zirconia anode in solid oxide fuel cells running on methane,* Catal. Today, 1998, 46, p.137

4. C. Mallon, K. Kendall, *Sensitivity of nickel cermet anodes to reduction conditions,*Journal of Power Sources, 145 (2005) 154-160

5. W.R. Grove, *Gas Voltaic Battery,* Philos. Mag 14, 1839,127

6. U.S Department of energy, *Fuel Cell Hand Book Version 5,* U.S. Department energy, National Energy Technology Laboratory, Morgantown, WV, 2000

7. M. Ormerod, *Solid Oxide Fuel Cells.* Chemical Soc. Rev, 2003. 32(1): p. 17-28.

8. C. Song, *Fuel processing for low-temperature and high-temperature fuel cells: Challenges, and opportunities for sustainable development in the 21st century.* Catalysis Today, 2002. 77(1-2): p. 17-49.

9. R.H. Song, S.N. Ryoo, *The present state and prospect of solid oxide fuel cell technology,* Pros. of ind. chemistry, 2004, **7**(2), 8-13.

10. J. Laminie and A.L. Dicks. *Fuel cell systems Explained*. Wiley, New York, 2000, 308

11. J.H. Hirschenhofer, D.B. Stauffer, R.R. Eagleman and M.G. Klett. Fuel cell hand book, 4th edn. DOE/FETC 99/1076, US Department of energy,

Fedral Energy Technology center, Morgantownm WV, Nov. 1998.

12. W.T. Grubb, Proceedings of the 11th annual battery research and development conference, PSC publications committee, Red bank, NJ, 5 P 1957, US Patent No 2,913,511, 1959

13. K. Prater, *The renaissance of the solid polymer fuel cell,* Journal of power sources, 1990, 29, p 239-250.

14. P.G. Gary and J. C Frost. *Impact on transportation*. Energ. Fuel. 1998, 12, p. 1121-1129.

15. S. Litster and G. Mclean, *PEM fuel cell electrodes,* Journal of power sources, 2004, 130(1-2), p. 61-76

16. A. Docter and A. Lamm. *Gasoline fuel cell system*. Journal of Power Sources, 1999, 84, 194- 200

17. J.C. Amphlett, M. Farahani, R.F. Mann, B.A. Peppley, P.R. Robrge, in proceedings of the 26th Intersociety energy conversion Engineering conference, 1991, 3, p 4-9, Conversion Technoilogy/Electrochemical conversion, American Nuclear Society, La Grange, Illinois, 1991, p. 624.

18. C.M. Finnerty and R. M. Ormerod, *Internal reforming over nickel/zirconia anodes in SOFCS operating on methane: influence of anode formulation, pre-treatment and operating conditions*, Journal of Power Sources, 2000 86(1-2), p. 390-394.

19. R.H. Song, *Micro SOFC technology*, News and information Chem. Eng., 2003, **21**(4), 478-483.

20. Andrew L. Dicks, *Molten carbonate fuel cells*, current opinion in solid state and materials science, 2004, 8(5), p 379-383.

21. J.H. Hirschenhofer, *Status of commercialization effort*, American power conference, Chicago, IL, April 1993.

22. N. Sammes, R. Bove and K Stahl, *Phosphoric acid fuel cells: fundamentals and applications*, Current opinion in solid state and materials science, 2004, 8(5), p 372-378.

23. H. Tu, and U. Stimming, *Advances, aging mechanisms and lifetime in solid-oxide fuel cells*. J. Power Sources, 2004, 127(1-2), p. 284-293.

24. K. Ahmed and K. Föger, in: Proceedings of the fourth European solid oxide fuel cell forum, 2000, 69**.**

25. R.H. Cunningham, et al., in: Proceedings of the fourth European solid oxide fuel cell forum, 2000, **77**.

26. A. Schuler, et al., in: Proceeding of the fourth European solid oxide fuel cell forum, 2000, 107**.**

27. S.M. Haile, *Fuel cell materials and components*, Acta Mat. 2003, 51(19), 5981-6000.

28. N.Q. Minh, T. Takahashi, *Science and technology of ceramic fuel cells*. Amsterdam; Elsvier; 1995.

29. W.Z. Zhu, and S.C. Deevi, *A review on the status of anode materials for solid oxide fuel cells.* Materials Science and Engineering A. Papers from the German Priority Programme (Functionally Graded Materials), 2003, 362(1-2): p. 228-239.

30. E. Lara-Curzio, T.R. Watkins, R. Trejo, C.R. Luttrell, M. Radovic, J. Lannutti, Et al., *Effect of temperature and H_2-induced reduction on the magnitude of residual stress in YSZ-NiO/YZS bi-layers*. In: 106th annual meeting and exposition of the American Ceramic Society, Indianapolis, 2004.

31. K. Kendall, M. Palin, *A small solid oxide fuel cell demonstrator for microelectronic applications.,* Journal of Power Sources, 1998, 71, p.268-270

32. R. Cunningham, C. Finnerty, K. Kendall, R.M. Ormerod, *A novel test system for in situ catalytic and electrochemical measurements on fuel processing anode in working solid oxide fuel cells,* Electrochem. Soc. Proc. 1997, 97(18), p. 965-972

33. J. Staniforth, K. Kendall, *Cannock landfill gas powering a small tubular solid oxide fuel cell — a case study,* Journal of Power Sources, 2000, 86, p. 401-403

34. S. Park, R. Cracium, J.M. Vohs, R.J. Gorte, *Direct oxidation of hydrocarbons in a solid-oxide fuel cell,* Journal of Electrochem. Soc., 1999, 146, p. 3603

35. J. Liu, B.D. Brian, Z.Q. Ji, S.A. Barnett, *Direct operation of solid oxide fuel cells with methane fuel,* Solid State Ionics, 2005 176(22-23), p. 1827-1835.

36. A.L. Dicks, *Hydrogen generation from natural gas for the fuel cell systems of tomorrow.* Journal of. Power Sources, 1996, 61(1-2), p. 113-124.

37. M. Brown, S. Primdahl, and M. Mogensen, *Structure/Performance Relations for Ni/Yttria-Stabilized Zirconia Anodes for Solid Oxide Fuel Cells.* Journal of The Electrochemical Society, 2000. 147(2), p. 475-485.

38. P.J. Gellings, and H.J.M. Bouwmeester, *Solid state aspects of oxidation catalysis.* Catalysis Today, 2000. 58(1): p. 1-53.

39. P.J. Gellings, and H.J.M. Bouwmeester, *Ion and mixed conducting oxides as catalysts.* Catalysis Today, 1992. 12(1): p. 1-101.

40. Y. Mizutani, et al., *From rare earth doped zirconia to 1 kW solid oxide fuel cell system,* Journal of Alloys and Compounds. Proceedings of Rare Earths'04 in Nara, Japan, 2006. 408-412: p. 518-524.

41. G. Dotelli, et al., *Composite materials as electrolytes for solid oxide fuel cells: simulation of microstructure and electrical properties,* Solid State Ionics, 2002. 152-153, p. 509-515.

42. S. Sarat, N. Sammes, and A. Smirnova, *Bismuth oxide doped scandia-stabilized zirconia electrolyte for the intermediate temperature solid oxide fuel cells.* Journal of Power Sources. Special issue including selected papers presented at the International Workshop on Molten Carbonate Fuel Cells and Related Science and Technology 2005

together with regular papers, 2006. 160(2), p. 892-896.

43. J.A. Kilner, and R.J. Brook, *A study of oxygen ion conductivity in doped nonstoichiometric oxides.* Solid State Ionics, 1982. 6(3), p. 237-252.

44. A.J. Appleby, *Fuel cell technology: Status and future prospects.* Energy, 1996. 21(7-8): p. 521-653.

45. L.J. Gauckler, et al., *Solid Oxide Fuel Cells: Systems and Materials.* CHIMIA International Journal for Chemistry, 2004, 58, p. 837-850.

46. N.Q. Minh, *Ceramic Fuel-Cells,* Journal of the American Ceramic Society. 1993, 76(3), p. 563-588.

47. T. Etsell, S. Flengas, *Electrical properties of solid oxide electrolytes,* Chemical Reviews, 1970, 70 (3), p. 339-376.

48. E. Subbarao, H. Maiti, *Solid electrolytes with oxygen ion conduction*, Solid State Ionics, 1984, 11 (4), p. 317-338.

49. S. Badwal, *Zirconia-based solid electrolytes - microstructures, stability and ionicconductivity*, Solid State Ionics, 1992, 52 (1-3), p 23-32.

50. S. Badwal, F. Ciacchi, D. Milosevic, *Scandia-zirconia electrolytes for intermediate temperature solid oxide fuel cell operation,* Solid State Ionics, 2000, 136, p. 91-99.

51. O. Yamamoto et al., *Electrical-conductivity of stabilized zirconia with ytterbia and scandia*, Solid State Ionics, 1995, 79, P. 137-142.

52. H. Inaba, and H. Tagawa, *Ceria-based solid electrolytes.* Solid State Ionics. 1996, 83(1-2): p. 1-16.

53. M. Dudek, *Ceramic oxide electrolytes based on CeO2--Preparation, properties and possibility of application to electrochemical devices.* Journal of the European Ceramic Society. Engineering Ceramics '07: From Engineering To Functionality, The Advanced Research Workshop Engineering Ceramics 2007, 2008, 28(5), p. 965-971.

54. J. Molenda, K. Swierczek, and W. Zajac, *Functional materials for the IT-SOFC.* Journal of Power Sources X Polish Conference on Systems with Fast Ionic Transport, 2007, 173(2), p. 657-670.

55. N.M. Sammes et al., *Bismuth based oxide electrolytes-- structure and ionic conductivity.* Journal of the European Ceramic Society, 1999, 19(10), p. 1801-1826.

56. R.L. Cook, R.C. MacDuff, and A.F. Sammells, *Perovskite Solid Electrolytes for Intermediate Temperature Solid Oxide Fuel Cells.* Journal of the Electrochemical Society, 1990, 137(10), p. 3309-3310.

57. T. Ishihara, et al., *Improved Oxide Ion Conductivity in $La_{0.8}Sr_{0.2}Ga_{0.8}Mg_{0.2}O_3$ by Doping Co,* Chem. Mater., 1999, 11(8), p. 2081-2088.

58. T. Ishihara, H. Matsuda, and Y. Takita, *Doped LaGaO3 Perovskite Type Oxide as a New Oxide Ionic Conductor,* Journal of Am. Chem. Soc., 1994. 116(9), p. 3801-3803.

59. S. Kim, et al., *Oxygen-ion conductivity of BaO- and MgO-doped LaGaO3 electrolytes.* Journal of Power Sources, 2001. 93(1-2): p. 279-284.

60. K. Nomura, and S. Tanase, *Electrical conduction behavior in (La0.9Sr0.1) MIIIO3-[delta] (MIII=Al, Ga, Sc, In, and Lu) perovskites.* Solid State Ionics, 1997. 98(3-4), p. 229-236.

61. T. –Y. Chen, R.-Y. Pan, and K.-Z. Fung, *Effect of divalent dopants on crystal structure and electrical properties of $LaAlO_3$ perovskite.* Journal of Physics and Chemistry of Solids, Proceedings of the 2nd International Symposium on Point Defect and Non-Stoichiometry (ISPN-2) - Proceedings of the 2nd International Symposium on Point Defect and Non-Stoichiometry (ISPN-2), 2008. 69(2-3), p. 540-546.

62. K. Kakinuma, et al., *Electrical conductivity and local distortion of (Ba0.5La0.5)2In2O5.5 doped with divalent or tetravalent cation in in-site.* Solid State Ionics, 2004. 168(1-2), p. 69-74.

63. J.B. Goodenough, J.E. Ruiz-Diaz, and Y.S. Zhen, *Oxide-ion conduction in Ba2In2O5 and Ba3In2MO8 (M=Ce, Hf, or Zr).* Solid State Ionics, 1990. 44(1-2), p. 21-31

64. K.R. Kendall, et al., *Recent developments in perovskite-based oxide ion conductors.* Solid State Ionics, 1995. 82(3-4), p. 215-223.

65. S. Nakayama, S. and M. Sakamoto, *Electrical properties of new type high oxide ionic conductor RE10Si6O27 (RE = La, Pr, Nd, Sm, Gd, Dy).* Journal of the European Ceramic Society, 1998. 18(10), p. 1413-1418.

66. S.P. Jiang and S.P.S Badwal, *Hydrogen Oxidation at the Nickel and Platinum Electrodes on Yttria-Tetragonal Zirconia Electrolyte,* Journal of Electrochem. Soc. 144, 1997, p. 3777-3784

67. M. Suzuki, H. Sakaki, S. Otoshi, A. Kajimura, M. Ippommatsu, *High power density solid oxide electrolyte fuel cells using Ru/Y_2O_3 stabilized zirconia cermet anodes,* Solid state Ionics, 62, 1993,p 125.

68. A. Atkinson et al., *Advanced anodes for high-temperature fuel cells.* Nature Materials, 2004, 3, p. 17–27.

69. S.P. Jiang, and S.H. Chan, *A review of anode materials development in solid oxide fuel cells,* Journal of Materials Science, 2004, 39(14), p. 4405-4439.

70. M. Mogensen and S. Skaarup, *Kinetic and geometric aspects of solid oxide fuel cell electrodes.* Solid State Ionics. Proceedings of the 10th International Conference on Solid State Ionics, 1996, 86-88(Part 2), p. 1151-1160.

71. B. De Boer et al., *The effect of the presence of fine YSZ particles on the performance of porous nickel electrodes.* Solid State Ionics, 2000, 127(3-4), p. 269-276.

72. Y. J. Leng, S. H. Chan, K. A. Khor, S. P. Jiang and P. Cheang, *Effect of characteristics of Y2O3/ZrO2 powders on fabrication of anode-supported solid oxide fuel cells*, Journal of Power Sources, 2003, 117(1-

2), P. 26-34.

73. H. Kim, S. Park, J.M. Vohs, R.J. Gorte, J, *Direct Oxidation of Liquid Fuels in a Solid Oxide Fuel Cell.* Electrochem. Soc. 2001, 148, A693-A695

74. T. Takeguchi, Y.Kani, T. Yano, R. Kikuchi, K. Eguchi, K. Tsujimoto, Y. Uchida, A. Ueno, K. Omoshiki, M. Aizawa, *Study on steam reforming of CH_4 and C_2 hydrocarbons and carbon deposition on Ni-YSZ cermets,* Journal of Power Sources. 2002, 112, p. 588-595

75. P. Holtappels, J. Bradly, J.T.S. Irvine, A. Kaier, M. Mogensen, *Disruption of extended defects in solid oxide fuel cell anodes for methane oxidation.* Journal of Electrochem. Soc. 2001, 148, p. A923-A929

76. O.A. Marina, C. Bagger, S. Primdahl, M. Mogensen, *A solid oxide fuel cell with a gadolinia-doped ceria anode: prepation and performance.* Solid State Ionics, 1999, 123, p. 199-208.

77. J.P. Van hook, *Methane-Steam Reforming.* Catal. Rev. Sci. Eng. 1980, 21, p. 1-51.

78. T. Takeguchi. R. Kikuchi, T. Yano, K. Eguchi, K. Murata, *Effect of precious metal addition to Ni-YSZ cermet on reforming of CH_4 and electrochemical activity as SOFC anode.* Catal. Today. 2003, 84, p. 217-222.

79. S. P. Simner, M. D. Anderson, J. E. Coleman and J. W. Stevenson, *Performance of a novel La(Sr)Fe(Co)O_3-Ag SOFC cathode*, Journal of Power Sources, 2006,

80. K. Kenjo, M. Nishiya, *LaMnO3 air cathodes containing ZrO2 electrolyte for high temperature solid oxide fuel cells*, Solid State Ionics. 1992, 57(3-4), p. 295-302

81. M.J.L. Østergård, C. Clausen, C. Bagger and M. Mogensen, *Manganite-zirconia composite cathodes for SOFC: Influence of structure and composition* Electrochem Acta. 1995, 40(12), p. 1971-1981

82. S. Carter et al., *Oxygen-transport in selected nonstoichiometric perovskite-structure oxides*, Solid State Ionics 1992, 53 (6), 597-60.

83. A. Hammouche, E. Siebert, A. Hammou, *Crystallographic, thermal and electrochemical properties of the system La1-xSrxMnO3 for high-temperature solid electrolyte fuel-cells*, Materials Research Bulletin, 1989, 24 (3), 367-380.

84. S. Singhal, *Advances in solid oxide fuel cell technology.* Solid State Ionics, 2000. 135(1-4): p. 305-313.

85. H. Uchida, S. Arisaka, and M. Watanabe, *High performance electrodes for mediumtemperature solid oxide fuel cells: Activation of La(Sr)CoO3 cathode with highly dispersed Pt metal electrocatalysts.* Solid State Ionics, 2000. 135(1-4), p. 347-351.

86. O. Yamamoto, et al., *Perovskite-type oxides as oxygen electrodes for high temperature oxide fuel cells.* Solid State Ionics, 1987, 22(2-3), p. 241-246.

87. A. Petric, P. Huang, and F. Tietz, *Evaluation of La-Sr-Co-Fe-O perovskites for solid oxide fuel cells and gas separation membranes.* Solid State Ionics, 2000, 135(1-4), p. 719-725.

88. J.M. Bae, and B.C.H. Steele, *Properties of Pyrochlore Ruthenate Cathodes for Intermediate Temperature Solid Oxide Fuel Cells.* Journal

of Electroceramics, 1999. 3(1) p. 37-46.

89. S. Wang, and Y. Zou, *High performance $Sm_{0.5}Sr_{0.5}CoO_3$-$La_{0.8}Sr_{0.2}Ga_{0.8}Mg_{0.15}Co_{0.05}O_3$ composite cathodes.* Electrochemistry Communications, 2006. 8(6), p. 927-931.

90. H. Fukunaga, et al., *Reaction model of dense Sm0.5Sr0.5CoO3 as SOFC cathode.* Solid State Ionics, 2000. 132(3-4) p. 279-285.

91. H. Lv, et al., *Effect of B-site doping on Sm0.5Sr0.5MxCo1-xO3-[delta] properties for IT-SOFC cathode material (M = Fe, Mn).* Materials Research Bulletin, 2007. 42(12), p. 1999-2012.

92. H.C. Yu, and K.-Z. Fung, *Electrode properties of La1-xSrxCuO2.5-[delta] as new cathode materials for intermediate-temperature SOFCs.* Journal of Power Sources, 2004. 133(2), p. 162-168.

93. C. Xia, et al., *Sm0.5Sr0.5CoO3 cathodes for low-temperature SOFCs.* Solid State Ionics, 2002. 149(1-2): p. 11-19.

94. Z. Yang, *Recent advances in metallic interconnects for solid oxide fuel cells.*International Materials Reviews, 2008. 53: p. 39-54.

95. F. Tietz, H.-P. Buchkremer, and D. Stover, *Components manufacturing for solid oxide fuel cells.* Solid State Ionics, 2002. 152-153: p. 373-381.

96. M.A.J Cropper, S. Geiger, and D.M. Jollie, *Fuel cells: a survey of current developments.* Journal of Power Sources, 2004. 131(1-2): p. 57-61.

97. N,Q Minh, *Solid oxide fuel cell technology--features and applications.* Solid State Ionics, 2004. 174(1-4): p. 271-277.

98. L. Groupp, and H.U. Anderson, *Densification of $La_{1-X}SRxcRo_3$.* Journal of the American Ceramic Society, 1976. 59(9-10): p. 449-450.

99. T. Nishi, N. Hisatome, H. Yamamoto and N. Murakami. In: P. Vincenzini (Ed.), proceedings of the 9th Cimtec World Forum on New Materials Innovative Materials in Advanced Energy Technologies 1999, 24, p. 41

100. G. Pudmich, B.A. Boukamp, M. Gonzalez-Cuenza, W. Jungen, W. Zipprich and F. tietz, *Chromite/titanate based perovskites for application as anodes in solid oxide fuel cells*, Solid State Ionics 2000, 135, 344

101. S. Linderoth, et al., *Investigations of metallic alloys for use as interconnects in solidoxide fuel cell stacks.* Journal of Materials Science, 1996. 31(19): p. 5077-5082.

102. D.M. England and A.V. Virkar**,** *Oxidation Kinetics of Some Nickel-Based Superalloy Foils in Humidified Hydrogen and Electronic Resistance of the Oxide Scale Formed Part II.* Journal of the Electrochemical Society, 2001. 148(4), p. A330-A338.

103. W.A. Meulenberg, et al., *Improved contacting by the use of silver in solid oxide fuelcells up to an operating temperature of 800 Â°C.* Journal of Materials Science, 2001. 36(13), p. 3189-3195.

104. F. Gardner et al., *SOFC technology development at Rolls-Royce*, Journal of Power Sources 2000, 86, p. 122-129.

105. M.C. Williams, J.P. Strakey and S.C. Singhal, U.S. distributed generation fuel cell program, Journal of power sources, 2004, 131(1-2), p. 79-85.

106. K. Kendall, (1992) *International Forum on Fine Ceramics* Japan Fine Ceramics Center, Nagoya Japan. P. 143 – 148

107. M. Kendall, *Tubular cells: a novel SOFC design,* Middlesex University, 1993

108. W. Bujalski, et al., *Cycling studies of solid oxide fuel cells.* Journal of Power Sources. Selected papers presented at the Ninth Grove Fuel Cell Symposium, 2006. 157(2), p. 745-749.

109. W. Bujalski, C.M. Dikwal, and K. Kendall, *Cycling of three solid oxide fuel cell types.* Journal of Power Sources. Scientific Advances in Fuel Cell Systems, Turin, Italy, 13-14 September 2006, 2007. 171(1), p. 96-100.

110. A. Weber, and E. Ivers-Tiffee, *Materials and concepts for solid oxide fuel cells (SOFCs) in stationary and mobile applications.* Journal of Power Sources. Eighth Ulmer Electrochemische Tage, 2004, 127(1-2), p. 273-283.

111. P. Aguiar, P., D.J.L. Brett, and N.P. Brandon, *Feasibility study and techno-economic analysis of an SOFC/battery hybrid system for vehicle applications.* Journal of Power Sources Scientific Advances in Fuel Cell Systems, Turin, Italy, 2006, 2007, 171(1), p. 186-197.

112. D.J.L, Brett, et al., *Concept and system design for a ZEBRA battery-intermediate temperature solid oxide fuel cell hybrid vehicle.* Journal of Power Sources. Selected papers presented at the Ninth Grove Fuel Cell Symposium, 2006, 157(2), p. 782-798.

113. D.J.L., Brett, P. Aguiar, and N.P. Brandon, *System modelling and integration of an intermediate temperature solid oxide fuel cell and ZEBRA battery for automotive applications.* Journal of Power Sources. Special issue including selected papers presented at the Second International Conference on Polymer Batteries and Fuel Cells together with regular papers, 2006, 163(1), p. 514-522.

114. E.V. Tsipis, V.V. Kharton and J.R. Frade, *Mixed conducting components of solid oxide fuel cell anodes*, Journal of the European Ceramic Society, 2005, 25(12), P. 2623-2626.

115. P.L. Eisele, *Characterization Of Material Behavior During The Manufacturing Process Of A Co-Extruded Solid Oxide Fuel Cell,* Georgia Institute of Technology, 2004

116. C.M. Dikwal, W. Bujalski, and K. Kendall, *Characterization of the electrochemical performance of micro-tubular SOFC in partial reduction and oxidation conditions,* Journal of Power Sources, 2008, 181(2), p. 267-273.

117. T. Alston, et al., *A 1000-cell SOFC reactor for domestic cogeneration.* Journal of Power Sources, 1998. 71(1-2), p. 271-274.

118. D. Waldbillig, A. Wood, and D.G. Ivey, *Thermal analysis of the cyclic reduction and oxidation behaviour of SOFC anodes.* Solid State Ionics, 2005. 176(9-10), p. 847-859.

119. D. Waldbillig, A. Wood, and D.G. Ivey, *Electrochemical and microstructural characterization of the redox tolerance of solid oxide fuel cell anodes.* Journal of Power Sources, Selected papers presented at the Fuel Cells Science and Technology Meeting, 2005, 145(2), p. 206-215.

120. J. Malzbender, E. Wessel, and R.W. Steinbrech, *Reduction and re-oxidation of anodes for solid oxide fuel cells.* Solid State Ionics, 2005. 176(29-30): p. 2201-2203.

121. J.N. Armor, *The multiple roles for catalysis in the production of H2.* Applied Catalysis A: General, 1999. 176(2), p. 159-176.

122. K. Kendall, *Hydrocarbon fuels: Hopes for a flame-free future.* Nature 2000. 404(6775), p. 233-235.

123. D.J.L Brett, et al., *Methanol as a direct fuel in intermediate temperature*

(500-) solid oxide fuel cells with copper based anodes. Chemical Engineering Science, 2005. 60(21), p. 5649-5662.

124. J. Meusinger, E. Riensche, and U. Stimming, *Reforming of natural gas in solid oxide fuel cell systems.* Journal of Power Sources, 1998. 71(1-2), p. 315-320.

125. K. Eguchi, et al., *Fuel flexibility in power generation by solid oxide fuel cells.* Solid State Ionics, 2002. 152-153, p. 411-416.

126. E. Achenbach and E. Riensche, *Methane/steam reforming kinetics for solid oxide fuel cells.* Journal of Power Sources, 1994. 52(2), p. 283-288.

127. E.P. Murray, T. Tsai, and S.A. Barnett, *A direct-methane fuel cell with a ceria-based anode.* Nature, 1999. 400(6745), p. 649-651.

128. A.L. Dicks, *Advances in catalysts for internal reforming in high temperature fuel cells.* Journal of Power Sources, 1998. 71(1-2), p. 111-122.

129. R. Peters, et al., *Internal reforming of methane in solid oxide fuel cell systems.* Journal of Power Sources, 2002. 106(1-2): p. 238-244.

130. J.H. Koh, et al., *Carbon deposition and cell performance of Ni-YSZ anode support SOFC with methane fuel.* Solid State Ionics, 2002. 149(3-4): p. 157-166.

131. K. Kendall, et al., *Effects of dilution on methane entering an SOFC anode.* Journal of Power Sources, 2002. 106(1-2): p. 323-327.

132. A.L. Dicks, K.D. Pointon, and A. Siddle, *Intrinsic reaction kinetics of methane steam reforming on a nickel/zirconia anode.* Journal of Power Sources, 2000. 86(1-2): p. 523-530.

133. J.L. Chambon, *New Energy Technologies*, in *Clefs CEA report*, Vol. 44, Paris, 2000, p.47.

134. Probstein and Hick, Synthetic fuels Mc Graw, Hill Book company, 1982

135. R. Ormerod, Internal reforming in solid oxide fuel cells, *Studies in Surface Science andCatalysis* 122, 35-46, 1999

136. I. Proctor, A. Hopkin, R. Ormerod, Development of anodes for direct electrocatalytic oxidation of methane in solid oxide fuel cells, *Ionics* 9 (3-4), 242-247, 2003

137. T. Hatae, N. Kakuda, T. Taniyama and Y. Yamazaki, *Low temperature preparation and performance of Ni/YSZ anode with a multi-layered structure for SOFC*, Journal of Power Sources, 2004, 135(1-2), p. 25-28.

138. T. Razpotnik and J. Macek, *Synthesis of nickel oxide/zirconia powders via a modified Pechini method*, Journal of the European Ceramic Society, 2006, 27 (2-3), p. 1405-1410.

139. H. Koide, Y. Someya, T. Yoshida and T. Maruyama, *Properties of Ni/YSZ cermet as anode for SOFC, Solid State Ionics*, 2000, 132(3-4), P. 253-260.

140. N. C. Triantafyllopoulos and S. G. Neophytides, *The nature and binding strength of carbon adspecies formed during the equilibrium dissociative adsorption of CH_4 on Ni-YSZ cermet catalysts*, Journal of Catalysis, 2003, 217(2), P. 324-333.

141. A. Dhir, and K. Kendall, *Microtubular SOFC anode optimisation for direct use on methane.* Journal of Power Sources, 2008. 181(2), p. 297-303.

142. T.J. Lee, and K. Kendall, *Characterisation of electrical performance of anode supported micro-tubular solid oxide fuel cell with methane fuel.* Journal of Power Sources, 2008. 181(2): p. 195-198.

143. K. Kendall, *Progress in solid oxide fuel cell materials.* International Materials Reviews, 2005. 50(5), p. 257-264.

144. G.J. Saunders, J. Preece, and K. Kendall, *Formulating liquid hydrocarbon fuels for SOFCs.* Journal of Power Sources, 2004. 131(1-2): p. 23-26. 205.

145. M. Lockett, M.J.H. Simmons, and K. Kendall, *CFD to predict temperature profile for scale up of micro-tubular SOFC stacks.* Journal of Power Sources, 2004. 131(1-2): p.243-246.

146. J. Latz, C. Mallon, and K. Kendall. (2004) *Operation of SOFCs with Nickel Cermet Anodes on Methane.* European Fuel Cell Forum, Lucerne / Switzerland. P. 369 – 377

147. G.J. Saunders, and K. Kendall, *Reactions of hydrocarbons in small tubular SOFCs.* Journal of Power Sources, 2002. 106(1-2): p. 258-263.

148. G.J. Saunders, *Reaction of Hydrocarbons in Zirconia Fuel cells,* University of Birmingham, 2002 PhD Thesis

149. A. Dhir, *Improved Microtubular solid oxide fuel cells,* University of Birmingham, 2008 PhD Thesis.

150. J. Preece, *Oxygenated hydrocarbon fuels for solid oxide fuel cells,* University of Birmingham, 2005 PhD Thesis

151. M. Radovic, E. Lara-Curzio, *Mechanical properties of tape cast nickel-based anode materials for solid oxide fuel cells before and after reduction in hydrogen,* Acta Materialia, 2004, 52, p. 5747-5756

152. Kwon, O.H. and G.M. Choi, *Electrical conductivity of thick film YSZ.* Solid State Ionics. Proceedings of the E-MRS Symposium P on Solid State Ionics: Mass and Charge Transport at Various Length Scales, 2006. 177(35-36): p. 3057-3062.

153. S.A. Barnett, Direct *hydrocarbon solid oxide fuel cells*, in: W. vielstich, A. Lamm, H. Gasteiger (Eds.), Handbook of Fuel Cell Technology, forth ed., Wiley, Hoboken, NJ, 2003, pp. 98-108.

154. S C Zhu, S.C. Deevi, *Materials science and Engineering*, A362, 228-239, 2003

155. B D. Madsen, S A. Barnett, *Effect of fuel composition in the performance of ceramic-based solid oxide fuel cell anodes.* Solid State Ionics, 2005, 176, P. 2545-2553

Publication

Journal of Power Sources

T.J. Lee, and K. Kendall, *Characterisation of electrical performance of anode supported micro-tubular solid oxide fuel cell with methane fuel.*, FUEL CELLS IN A CHANGING WORLD SELECTED PAPERS FROM THE TENTH GROVE FUEL CELL SYMPOSIUM 2008. 181(2): p. 195-198.